Divergent downstream biosynthetic pathways are supported by L-cysteine synthases of *Mycobacterium tuberculosis*

Mehak Zahoor Khan[1,2], Deborah M. Hunt[3], Biplab Singha[1,2], Yogita Kapoor[2,6], Nitesh Kumar Singh[2], D. V. Sai Prasad[4], Dharmarajan Sriram[4], Divya Tej Sowpati[2], Luiz Pedro S. de Carvalho[3,5,#], Vinay Kumar Nandicoori[1,2,6#]

[1] National Institute of Immunology, New Delhi, 110067, India

[2] CSIR-Centre for Cellular and Molecular Biology, Hyderabad, 500007, India

[3] The Francis Crick Institute, 1 Midland Road, London, NW1 1AT, United Kingdom

[4] Department of Pharmacy, Birla Institute of Technology and Science-Pilani, Hyderabad Campus, Jawahar Nagar, Hyderabad, 500078, India

[5]Department of Chemistry, The Herbert Wertheim UF Scripps Institute for Biomedical Innovation & Technology, 130 Scripps Way, Jupiter FL 33458, United States

[6.] Academy of Scientific and Innovative Research (AcSIR), CSIR-Centre for Cellular and Molecular Biology (CSIR-CCMB) Campus, Hyderabad, 500007, India

[#]Address correspondence to: vinaykn@nii.ac.in & vinaykn@ccmb.res.in;
luiz.carvalho@crick.ac.uk & soriodecarval.lp@ufl.edu

Keywords: mycobacteria, tuberculosis, metabolism, cysteine synthases, redox, ROS, RNS

Running title: Non-redundant roles of non-canonical cysteine synthases in *M. tuberculosis*

Abstract

Mycobacterium tuberculosis's (Mtb) autarkic lifestyle within the host involves rewiring its transcriptional networks to combat host-induced stresses. With the help of RNA-seq performed under various stress conditions, we identified that genes belonging to *Mtb* sulfur metabolism pathways are significantly upregulated during oxidative stress. Using an integrated approach of microbial genetics, transcriptomics, metabolomics, animal experiments, chemical inhibition, and rescue studies, we investigated the biological role of non-canonical L-cysteine synthases, CysM and CysK2. While transcriptome signatures of *RvΔcysM* and *RvΔcysK2* appear similar under regular growth conditions, we observed unique transcriptional signatures when subjected to oxidative stress. We followed pool size and labelling (^{34}S) of key downstream metabolites, viz. mycothiol and ergothioneine, to monitor L-cysteine biosynthesis and utilization. This revealed the significant role of distinct L-cysteine biosynthetic routes on redox stress and homeostasis. CysM and CysK2 independently facilitate *Mtb* survival by alleviating host-induced redox stress, suggesting they are not fully redundant during infection. With the help of genetic mutants and chemical inhibitors, we show that CysM and CysK2 serve as unique, attractive targets for adjunct therapy to combat mycobacterial infection.

Introduction

Mycobacterium tuberculosis (Mtb) continues to stride as the number one killer among all infectious diseases, accounting for nearly 1.5 million deaths yearly. The aggravating situation is despite the clinical use of over 20 antibiotics and a century-old vaccine, BCG. The gradual rise in the emergence of increasingly drug-resistant strains and HIV-TB co-infection further highlights the urgency to identify newer attractive drug targets. Throughout the course of infection, *Mtb* is exposed to a continuum of dynamic host-induced stresses such as severe nutrient deprivation, acidified compartments, and toxic reactive oxygen species (ROS) and reactive nitrogen species (RNS) produced by its resident phagosomes. In turn, *Mtb* produces copious amounts of actinomycetes-specific mycothiol, the major antioxidant in actinomycetes that act as the functional equivalent of glutathione, to combat ROS and RNS. In addition to mycothiol, *Mtb* also produces ergothioneine, a low molecular weight thiol, and several enzymes that act concertedly to subvert host-induced redox stress. The redox-active group of both mycothiol and ergothioneine is derived from L-cysteine. Hence, genes involved in the biosynthesis of L-cysteine are upregulated in the host and *in vitro* upon oxidative and nutritional stress [1-5]. Notably, an increased expression of these genes is functionally crucial, as suggested by the attenuated survival of transposon mutants of many sulfur and L-cysteine biosynthesis genes within the host [6]. In mycobacteria, sulfur assimilation begins with the import of sulfate through a sulfate transporter composed of SufI.CysT.W.A. Intracellular sulfate is a substrate for APS synthase CysD.N.C, which adenylates and phosphorylates sulfate to form adenosine 5′-phosphosulfate (APS) [7-9]. APS sits at a metabolic branch point; it can either be converted into sulfolipids [10] by consequent actions of multiple Stfs enzymes or reduced via SirA and SirH to sulfide (Figure S1). This pathway encompasses sulfide formation from sulfate, called the sulfur assimilation pathway [11, 12] *Mtb* genome encodes three L-cysteine synthases – the canonical CysK1 and non-canonical CysM and CysK2 enzymes. Interestingly, humans do not possess L-cysteine synthases, raising the possibility of developing antibiotics without a homologous target in the host. CysK1 utilizes sulfide produced via the sulfur assimilation pathway and O-acetyl-L-serine produced from glycolytic intermediate 3-phosphoglycerate to produce L-cysteine [13-18] CysM, on the other hand, uses O-phospho-L-serine and a small sulfur carrier protein CysO as substrates [15, 18]. Like CysK1, CysK2 utilizes O-phospho-L-serine and sulfide as substrates [19, 20] (Figure S1). In addition, *Mtb* can also synthesize L-cysteine through a reverse transsulfuration pathway from L-methionine. This example of convergent metabolic redundancy raises several interesting questions: (1) Why would *Mtb* rely on multiple enzymes and pathways to produce the same biomolecule? (2) Are these "functionally redundant" enzymes dispensable, or are they

required at a distinct cellular space, time, and condition? (3) Is the L-cysteine pool produced through a particular pathway functionally compartmentalized? That is, is it metabolized into a specific kind of downstream thiol?

To define these unsolved aspects of *Mtb* L-cysteine metabolism, we sought to investigate the interplay of non-canonical L-cysteine synthases of *Mtb* and elucidate their roles in abetting virulence. We aimed to decipher the relative contribution of CysM and CysK2 enzymes in alleviating host-induced stresses and promoting the survival of *Mtb* within the host. We also investigated their role in secondary metabolism, synthesizing low molecular weight thiols, such as mycothiol and ergothioneine, and understanding the consequential effects of their deletion on the global transcriptome of *Mtb.* Lastly, with the help of specific inhibitors, we evaluated their potential to serve as attractive drug targets for adjunct antibiotic therapy.

Results

Non-canonical L-cysteine synthases facilitate Mtb in combating host-induced stresses.

Mtb is a generalist, a prototroph organism that can produce all 20 proteinogenic amino acids. In agreement with this notion, numerous microarray studies depict the upregulation of multiple amino acid pathways within the host [3, 4, 12], indicating a higher dependency of *Mtb* survival and virulence on amino acid biosynthesis and regulation. In response to infection, host immune responses often try to contain the bacillary growth by depriving the amino acid levels in intracellular environment. As a counter mechanism, *Mtb* has been shown to upregulate biosynthesis of amino acids such as tryptophan, lysine, and histidine to facilitate mycobacterial survival within the host [21, 22]. We sought to identify distinct host stresses that result in the transcriptional modulation of specific amino acid biosynthetic pathways with the help of RNA sequencing (RNA-Seq). We compared the transcriptional profile of *H37Rv* (*Rv*) grown in 7H9-ADC with the profiles obtained when bacilli were subjected to oxidative, nitrosative, starvation, and acidic stresses (Table S1). The volcano plot illustrates differentially expressed genes (DEGs) that were significantly upregulated (blue) and downregulated (red) under indicated stress conditions (absolute $\log_2$ Fold change>1 and Padj<0.05) (Figure S2a-e). Exposure to starvation conditions resulted in drastic transcription modulation compared with other stresses, suggesting that nutrient deficiency is the primary driver of transcriptome remodelling. In contrast, we observed the lowest number of DEGs when the bacteria were subjected to mildly acidic conditions (pH 5.5). Heat maps of normalized DEGs depict that DEG changes were comparable across biological replicates within each sample set (Figure S2f-j). To better understand the RNA-seq results, we plotted the fold change of differentially expressed genes due to different stress conditions (Figure S3 & Table S2). This allowed us to understand the expression profile of genes in all the stress conditions simultaneously, regardless of whether they were identified as differentially expressed. The data revealed that specific clusters of genes are up- and downregulated in oxidative, SDS, and starvation conditions. In comparison, the differences observed in the pH 5.5 and nitrosative conditions were limited (Figure S3 & Table S2).

To further refine our understanding of the DEGs, we grouped them into various functional categories and found that genes belonging to intermediary metabolism & respiration remained the most affected in all conditions highlighting their role of metabolic rewiring (Figure S4a). Pathway enrichment analysis of the most enriched Gene Ontology (GO) further revealed that, while,

expectedly, metabolic pathways were found to be downregulated during starvation, we observed enrichment of nitrogen metabolism (Figure S4b & Table S3). SDS stress resulted in the upregulation of branched-chain amino acids/keto acids degradation pathways (Figure S4c), and nitrosative stress ensued up-regulation of fatty acid and lipid biosynthetic processes (Figure S4d). There were no changes observed in mildly acidic conditions (Figure S4e). Importantly, oxidative stress resulted in significant up-regulation of genes involved in sulfur metabolism (Figure S4f). We further analyzed the DEGs involved in sulfur and L-cysteine metabolism across sample sets and discerned an overlap of the genes affected under two or more conditions. Interestingly, we observed upregulation of sulfate transporters genes (*subI*, *cysT*, *cysW*, *cysA1*) across multiple stresses and sulfur assimilation (*cysH, cysA2, cysD, cysNC)* during starvation, oxidative and SDS stress. *CysK2*, a non-canonical L-cysteine synthase, was found to be up-regulated during all stresses except SDS stress (Figure 1a).

Thus RNA-Seq data suggest that genes involved in sulfur assimilation and L-cysteine biosynthetic pathway are upregulated during various host-like stresses in *Mtb* (Figure S4). Given the importance of sulphur metabolism genes in *in vivo* survival of *Mtb* [23, 24] it is not surprising that diverse environment cues dynamically regulate these genes. Microarray studies have shown upregulation of genes encoding sulphate transporter upon exposure to hydrogen peroxide and nutrient starvation [1, 4, 25-27]. Similarly, ATP sulfurylase and APS kinase are induced during macrophage infection and by nutrient depletion. Induction of these genes that coordinate the first few steps of the sulphur assimilation pathway indicates a probable increase in biosynthesis of sulphate-containing metabolites that may be crucial against host-inflicted stresses. Furthermore, genes involved in synthesis of reduced sulphur moieties (*cysH*, *sirA* and *cysM*) are also induced by hydrogen peroxide and nutrient starvation. Sulfur metabolism has been postulated to be important in transition to latency. This hypothesis is based on transcriptional upregulation of *cysD*, *cysNC*, *cysK2*, and *cysM* upon exposure to hypoxia. Multiple transcriptional profiling studies have reported upregulation of *moeZ*, *mec*, *cysO* and *cysM* genes when cells were subjected to oxidative and hypoxic stress [2, 18, 23, 26-29] further suggesting an increase in the biosynthesis of reduced metabolites such as cysteine and methionine and sulfur containing cell wall glycolipids upon exposure to oxidative stress. To address the functional relevance of this observation, we deleted two non-canonical L-cysteine synthases-CysM [5] and CysK2, from the *Mtb* chromosome. CysK2 mutant, *RvΔcysK2,* was generated using the recombineering method, and the recombination at the native loci was confirmed with the help of multiple PCRs (Figure 1b). While deletion of *cysM* or *cysK2* did not affect mycobacterial growth under *in vitro* nutrient-rich 7H9-ADC or 7H9-ADS

(Figure S5a and S5b), it significantly compromised *Mtb* growth in defined Sauton's media (~2 $\log_{10}$; Figure 1c), suggesting the importance of *cysM*- and *cysK2*-derived L-cysteine. Restoring *cysM* or *cysK2* expression in the complementation strains, *RvΔcysM::M* and *RvΔcysK2::K2,* rescued the growth defects (Figure S5 & Figure 1c). *Mtb* is a metabolically versatile organism capable of utilizing a large variety of carbon and nitrogen sources [30]. Unlike 7H9, wherein glucose, glycerol, glutamate, and ammonia act as carbon and nitrogen sources, Sauton's media contains glycerol and asparagine as the sole carbon and nitrogen sources, suggesting metabolic reprogramming aided by CysM and CysK2 enable *Mtb* to grow optimally in a limited nutritional environment. This observation was further recapitulated under nutrient starvation (PBS), wherein the survival of *RvΔcysM* and *RvΔcysK2* was lower than parental *Rv* or *RvΔcysM::M* or *RvΔcysK2::K2* strains (Figure 1d). Interestingly, when exposed to acidic conditions (pH 4.5), *RvΔcysM* and *RvΔcysK2* survival were observed to be ~0.85 and ~0.24 $\log_{10}$ lower, respectively, compared with *Rv*, suggesting CysM is relatively more important for bacillary survival under acidic stress (Figure 1e). The highest attenuation of *RvΔcysM* and *RvΔcysK2* was observed upon the addition of cumene hydroperoxide (CHP), an organic hydroperoxide that, upon decomposition, generates free radicals. The relative survival of *RvΔcysM* and *RvΔcysK2* was ~2.04 and ~1.31 $\log_{10}$ lower, respectively, compared to *Rv* (Figure 1f). The addition of diamide, which results in thiol oxidation, also attenuated the survival of *RvΔcysM* and *RvΔcysK2* by ~1.33 and ~1.26 $\log_{10}$ compared with *Rv* (Figure S5c). When the mutant strains were subjected to nitrosative stress, the survival of *RvΔcysM* and *RvΔcysK2* was ~0.93 and ~0.86 $\log_{10}$ lower than *Rv* (Figure 1g). However, no significant attenuation was found during reductive and SDS stress (Figure 1h-i). Collectively, *RvΔcysM* and *RvΔcysK2* displayed increased susceptibility towards oxidative, nitrosative, mild acidification, and PBS starvation to varying degrees compared with *Rv, RvΔcysM::M* and *RvΔcysK2::K2*. The data suggests that L-cysteine, produced via CysM and CysK2, and its downstream products help mycobacteria thwart specific stresses that *Mtb* encounters within the host.

Distinct roles of CysM and CysK2.

To decipher the mechanism through which CysM and CysK2 combat oxidative stress, we performed a global transcriptomic analysis of *Rv*, *RvΔcysM*, and *RvΔcysK2* in the presence and absence of oxidative stress (CHP) (Table S4). Principal Component Analysis demonstrated clear separation of strains under different conditions. Intriguingly, while *RvΔcysM* and *RvΔcysK2* were closely located on a PCA plot in the absence of any stress, oxidative stress resulted in a significant divergence between the two groups (Figure 2a). Deletion of *cysM* resulted in differential expression of 322 genes (159 downregulated and 163 upregulated) (Figure S6a-b), while deletion of *cysK2*

impacted 278 genes (155 downregulated and 123 upregulated) under regular growth conditions (Figure S6c-d) (absolute $\log_2$ Fold change>1 and Padj<0.05). In contrast, upon treatment with CHP, nearly ~33% and ~53% of *Mtb* genes were differentially expressed in *RvΔcysM* and *RvΔcysK2,* respectively, compared with *Rv* (Figure 2b-c). To understand the individual contribution of CysM and CysK2 in combating oxidative stress, we compared the DEGs of *RvΔcysK2* to *RvΔcysM* under regular growth and oxidative stress conditions. While DEGs between *RvΔcysK2* and *RvΔcysM* were limited to 13 in untreated conditions (Figure 2d), CHP treatment resulted in differential expression of 1372 genes (Figure 2e and Figure S6e), highlighting unique transcriptional signatures associated with each L-cysteine synthase under oxidative stress. Subsequently, we compared the DEGs of *Rv*, *RvΔcysM*, and *RvΔcysK2* obtained under oxidative stress with the help of a Venn diagram. This analysis revealed that CysM and CysK2 influence a shared repertoire of 1023 genes (529 upregulated and 494 downregulated) compared to *Rv* upon CHP treatment (Figure 2f). Importantly, CysM and CysK2 distinctively modulate 324 and 1104 genes, respectively, during oxidative stress (Figure 2f-g). In addition to being directly regulated by the synthases, it is highly that the changes in the expression of these genes is because of distinct downstream consequences. Assortment of DEGs into functional classes revealed intermediary metabolism & respiration and cell wall pathways among the most impacted categories (Figure 2h). These results corroborate the recent finding that CysK2 alters the phospholipid profile of the *Mtb* cell envelope [31]. Pathway enrichment analysis of the most enriched Gene ontology biological process indicated that while most pathways are commonly affected by CysM and CysK2, these L-cysteine synthases also have a unique transcriptional footprint (Table S5). Pathways such as DNA binding, homologous recombination, translation, ribosome, etc., were commonly affected in *RvΔcysM* and *RvΔcysK2* compared to *Rv* during oxidative stress (Figure S6f, g). Genes belonging to oxidative phosphorylation and quinone binding were upregulated, while DNA binding and cholesterol catabolism gene categories were found to be downregulated in *RvΔcysM* compared to *RvΔcysK2* during oxidative conditions (Figure 2i). Together, our data point to the unique roles of CysM and CysK2, as their deletion differentially affects various cellular pathways under oxidative stress.

Key metabolites are differentially affected upon CysM and CysK2 deletion.

L-Cysteine concentration in *Mtb* is notoriously low, usually 10-fold lower than most other amino acids [32]. As expected, L-cysteine levels were below the limit of detection/quantification (not shown). Therefore, we used key downstream metabolites to monitor L-cysteine biosynthesis and utilization. We followed pool size and labelling ($Na^{34}SO_4$) of L-methionine, mycothiol/mycothione, and ergothioneine, made from L-cysteine, via three distinct and dedicated

metabolic pathways (Figure S7). First, L-methionine, mycothiol, and ergothioneine concentrations vary from zero to 24 h, indicating that their pool sizes are not as stable as those of other core metabolites. This is consistent with their function, susceptibility to redox homeostasis, and L-methionine's role in protein synthesis. Second, upon challenge with CHP for 24 h, L-methionine levels decrease in *Rv*, remain constant in *RvDcysK2*, and increase in *RvDcysM* (Figure 3a). Ergothioneine levels are identical in the three strains, and upon treatment with CHP, they are decreased in the parent strain but remain unchanged in the *RvDcysK2* and *RvDcysM* mutant (Figure 3b). Mycothiol levels increase in the *Rv*, *RvDcysK2* strains and remain nearly constant in *RvDcysM* (Figure 3c). Finally, mycothione levels increased slightly in the parent strain, decreased in the *RvDcysK2*, and remained stable in the *RvDcysM* strain (Figure 3d). These changes revealed a significant role of distinct L-cysteine biosynthetic routes on redox stress and homeostasis.

Employing ^{34}S labelling, we observed a reduced rate of synthesis of mycothiol, mycothione and ergothioneine in *RvΔcysM* compared to *Rv* and *RvΔcysK2* (Figure 3e-g). Interestingly, ergothioneine levels were found to be reduced in both *RvΔcysM* and *RvΔcysK2* compared to *Rv,* possibly underlying one of the reasons for their enhanced sensitivity to oxidative stress.

This result further indicates that these two routes are partially redundant; that is, they generate the same end product, L-cysteine. Yet, pool size measurements demonstrate significant changes, highlighting that while these pathways produce the same metabolite, their complex biological roles and requirements (co-substrates, pathways, regulation, etc.) are not fully redundant. This interpretation is in accordance with transcriptomics and phenotypic results described above. These non-overlapping metabolic requirements (*e.g.*, O-acetyl-L-serine vs. O-phospho-L-serine vs. CysM) are likely the source of the different metabolic phenotypes observed. Therefore, even producing the same end-product, genetic disruption of different L-cysteine synthases differently affects bacterium metabolism and fitness, leading to the distinct phenotypes observed between *RvDcysK2* and *RvDcysM in vitro*, *in cellulo*, and *in vivo*.

CysM and CysK2 alleviate the toxicity of host-produced ROS and RNS.

To define whether the attenuation of mutant strains observed during defined *in vitro* host-like conditions can be recapitulated within the host cells, we compared the survival of parental, mutants, and complementation strains in murine peritoneal macrophages (Figure 4a). Survival of *RvΔcysM* and *RvΔcysK2* was ~1.22 and ~0.85 $\log_{10}$ lower, respectively, compared with *Rv* at 96 h post-infection (p.i) (Figure 4b). Notably, the addition of L-cysteine alleviated survival differences (Figure 4c), suggesting that reduced L-cysteine levels in mutant strains are responsible for their attenuated survival. To further validate that CysM and CysK2 support *Mtb* survival by detoxifying

peroxides generated by the host, we compared the survival of strains in the peritoneal macrophages extracted from wild-type C57BL/6 (WT) mice that are proficient in eliciting oxidative and nitrosative stress or murine strains that are deficient in their ability to produce hydrogen peroxide (H_2O_2) (phox$^{-/-}$) or both oxidative and nitrosative stress (IFNγ$^{-/-}$). As anticipated, regardless of the mice genotype, there was no difference in the survival of *Rv* and complementation strains (Figure 4d-e). On the other hand, attenuation of *RvΔcysM* and *RvΔcysK2* observed in wild-type macrophages is partially reversed in the macrophages obtained from phox$^{-/-}$ mice (Figure 4d) and completely nullified in macrophages isolated from IFNγ$^{-/-}$ mice (Figure 4e). To further dissect the relative contribution of CysM and CysK2 in combating ROS and RNS independently or collectively, the survival of *Mtb* strains was examined in peritoneal macrophages isolated from WT and phox$^{-/-}$ in the presence or absence of iNOS inhibitor. While the inhibition of ROS or RNS independently only partially alleviated the attenuated survival *RvΔcysM* and *RvΔcysK2*, inhibition of both ROS and RNS by treating peritoneal macrophages isolated from phox$^{-/-}$ with iNOS inhibitor completely nullified survival defects of the mutants (Figure 4f). These results suggest that non-canonical L-cysteine synthases, CysM and CysK2, play an essential role in combating host-induced redox stress.

CysM and CysK2-derived L-cysteine support mycobacterial survival in vivo.

Given the importance of non-canonical L-cysteine synthases in mitigating host-induced redox stress, we next sought to examine whether CysM and CysK2 independently facilitate mycobacterial survival in a murine infection model. We followed disease progression by enumerating colony forming units (CFU) of the lung and spleen of the infected mice at day 1, 4, and 8 weeks p.i (Figure 5a & d). CFUs enumerated on day 1 showed equal bacillary deposition across strains in the lungs (Figure 5b & e). Compared with *Rv*, survival of *RvΔcysM* was ~1.25 $\log_{10}$ lower at 4 weeks p.i, which further attenuated to ~1.71 $\log_{10}$ at 8 weeks p.i in the lungs (Figure 5b). Similarly, dissemination of *RvΔcysM* in the spleen was ~1.63 $\log_{10}$ lower at 4 weeks p.i and ~1.72 $\log_{10}$ lower at 8 weeks p.i compared with *Rv* (Figure 5c). Similarly, *RvΔcysK2 was* ~1.67 $\log_{10}$ and ~1.87 $\log_{10}$ lower at 4 and 8 weeks p.i, respectively, compared with *Rv* in the lungs (Figure 5e) and ~1.63 $\log_{10}$ and ~1.72 $\log_{10}$ lower at 4 and 8 weeks p.i, respectively in the spleens of infected mice (Figure 5f).

To understand whether the ability of CysM to mitigate oxidative and nitrosative stress is linked to its role in facilitating mycobacterial survival *in vivo,* we infected WT, phox$^{-/-}$ and IFNγ$^{-/-}$ mice with *Rv*, *RvΔcysM* and *RvΔcysM::M* and analyzed bacillary load at 4 weeks p.i (Figure 5g). As shown in Figures 5h & 5i, the survival of *RvΔcysM* is impaired in WT mice that produce both ROS

and RNS, compared with phox$^{-/-}$ and IFNγ$^{-/-}$ mice. The survival defect observed due to the absence of CysM in the lungs was partially rescued in phox$^{-/-}$ mice. Due to the lack of ROS and RNS in IFNγ$^{-/-}$ mice, *RvΔcysM* showed higher bacillary load than in phox$^{-/-}$ mice (Figure 5h). *RvΔcysM* displayed better survival in phox$^{-/-}$ and IFNγ$^{-/-}$mice in the spleen than lungs, which could either be because of relatively lesser ROS and RNS stress or imperiled response in clearing *Mtb* infection (Figure 5i). In contrast to the peritoneal macrophage infection experiment (Figure 4), attenuated survival of *RvΔcysM* was not completely salvaged in IFNγ^{-}/$^{-}$ mice, suggesting that CysM may also be involved in alleviating additional stresses such as nutrient deprivation and/or IFNγ independent ROS/RNS produced by the host. Data presented suggests that L-cysteine produced through non-canonical pathways are independently important for mycobacterial survival *in vivo*.

***L-Cysteine synthase inhibitors can effectively kill Mtb* within the host.**

Data presented above demonstrated that CysM and CysK2 might serve as clinically-important targets for adjunct TB therapy. Brunner *et al.* screened a compound library to identify inhibitors of mycobacterial L-cysteine synthases- CysK1, CysK2, and CysM. We selected three compounds - Compound 1 (C1) (named compound 2 in [28]), which inhibits all three synthases; Compound 2 (C2) (compound 6 in [28]), which inhibits both non-canonical L-cysteine synthases and Compound 3 (C3) (compound 31 in [28]), which selectively inhibits CysK1 (Figure 6a & b). To examine the therapeutic potential of these inhibitors, we first tested their effect on the survival of *Rv* within host peritoneal macrophages. Treatment with C1 resulted in ~1 $\log_{10}$ attenuation compared with the untreated cells. Killing mediated by C2 or C3 was marginally lower compared with C1 (Figure 6c). Next, we examined the ability of these drugs to enhance the bactericidal activity of INH, a drug whose activity depends on redox state of the cell [33], and therefore could be affected by disruption of L-cysteine downstream pathways. Towards this goal, we first measured the MICs of INH (0.06 μg/ml) and C1 (0.6 mg/ml), C2 (0.6 mg/ml), and C3 (0.15 mg/ml) independently. As expected, all the compounds were ineffective in killing *Mtb* because of redundant roles and relatively less requirement of L-cysteine synthases during regular growth conditions. To examine the combinatorial effect, we selected sub-MIC values of INH (0.03 μg/mL, encircled orange) and increasingly two-fold diluted concentrations of C1, C2, or C3, all below MIC values (Figure 6d-f; blue encircled denotes the starting concentration) and assessed bacterial survival upon combinatorial treatment with INH and the three L-cysteine synthase inhibitors. The addition of either of the inhibitors below MIC rendered *Mtb* highly susceptible to INH, highlighting the potency of these compounds to serve as an adjunct therapy to combat mycobacterial infection.

Discussion

Throughout its course of infection, *Mtb* must persist in a hostile, oxidizing, and nutrient-deprived environment of host macrophage. Understanding the dynamic metabolic interactions between the pathogen and its host is imperative to identify its weaknesses which can be exploited to design new-age chemotherapy. Our study provides convincing evidence that the genes involved in the L-cysteine biosynthetic pathway are attractive targets for the design of anti-mycobacterial drugs. Genes involved in sulfur assimilation and L-cysteine biosynthesis were found to be upregulated in the transcriptome profile of *Rv* subjected to various host-like stresses. The sulfur metabolism pathway was particularly enriched upon the addition of oxidizing agent, CHP (Figure 1, S2 & S3). This observation has been consistently reported by multiple studies demonstrating the up-regulation of sulfur assimilation and L-cysteine biosynthetic genes in response to oxidative stress, nutrient deprivation, and macrophage infection [1-5]. Besides being involved in protein synthesis, L-cysteine is also important for the biosynthesis of L-methionine, S-adenosyl methionine, coenzyme A, and iron-sulfur clusters. As a thiol-containing molecule, L-cysteine contributes to the intracellular redox state directly and through the production of major antioxidants like mycothiol and ergothioneine. These numerous essential functions of L-cysteine prompted us to further examine its roles in the context of *Mtb* cellular metabolism and virulence.

Unlike *Mtb*Δ*cysH*, which was reported to be an L-cysteine auxotroph and thus required L-methionine or glutathione supplementation to grow *in vitro* (from which L-cysteine can be generated catabolically)[24], neither deletion of *cysK2* nor *cysM* impacted *Mtb* growth kinetics *in vitro* suggesting that these genes are functionally redundant during rich growth conditions [5] [31] (Figure S5). Interestingly, the induction of various host-like stresses attenuated the growth of these mutants compared to the parental strain, pointing towards the possibility of an enhanced requirement of L-cysteine-derived antioxidants and other biomolecules to subvert these stresses (Figure 1). In agreement with this hypothesis, we previously showed that the cellular thiol levels are higher during oxidative stress in *Mtb* [5]. Similarly, various MSH and ERG mutants display enhanced sensitivity to oxidative stress caused by treatment with H_2O_2, cumene hydroperoxide, or $O_2^{\bullet-}$ [34-38].

While the transcriptomic profiles of mutants were highly similar to each other during regular growth conditions, the addition of CHP resulted in differential expression of >30% *Mtb* genes, indicating that cues and downstream effects of the two non-canonical L-cysteine synthases are partially non-overlapping, further underlying their importance for the bacillary growth inside the host (Figure 2). We also found that the steady-state levels (pool sizes) of key L-cysteine derived

antioxidants, ergothioneine, and mycothiol, are significantly different at 24 h (Figure 3). The rate of synthesis of mycothiol, mycothione and ergothioneine were observed to be lower in *RvΔcysM* compared to *Rv* and *RvΔcysK2.*

The addition of L-cysteine in oxidatively stressed cells nullified the compromised survival of the mutants indicating that *Mtb* cells are able to uptake L-cysteine from the extracellular medium, as shown previously [5], and reduced levels of L-cysteine in the mutants are chiefly responsible for their attenuated growth in the presence of stresses (Figure 4). Various *Mtb* mutants in mycobacterial sulfur metabolism genes are severely compromised to persist within the host and cause disease [24, 39-44]. Inorganic sulfate is present at 300-500 μM in human plasma [44]. However, the inability of host-derived sulfur/L-cysteine to compensate for attenuated survival of mutants is suggestive of either inaccessibility of sufficient L-cysteine in *Mtb* niches or inefficient expression, function, or uptake by transporters *in vivo*. Importantly, compromised survival of *RvΔcysM* and *RvΔcysK2 in vivo* was largely mitigated in IFNg-/- and Phox-/-, indicating that the non-canonical L-cysteine synthases, CysM and CysK2, independently facilitate mycobacterial survival during immune-mediated redox stress (Figure 5).

Using network analysis of the *Mtb* protein interactome, a flux balance analysis of the reactome and randomized transposon mutagenesis data, along with sequence analyses and a structural assessment of targetability, Raman *et al.,* reported CysK2 and CysM as high confidence drug targets [45]. Similarly, inhibitors of CysM showed mycobactericidal activity in a nutrient-starvation model of dormancy [46]. Interestingly, humans do not reduce sulfur to produce L-cysteine; they rather synthesize L-cysteine through SAM-dependent transmethylation followed by transsulfuration of L-methionine. Owing to their complete absence in humans, mycobacterial L-cysteine biosynthetic genes and their regulators represent unique, attractive targets for therapeutic intervention [47]. We found that both *RvΔcysM* and *RvΔcysK2* displayed enhanced antibiotic sensitivity *in vitro* and within the host (data not shown). Importantly, a combination of L-cysteine synthase inhibitors with front-line TB drugs like INH, significantly reduced the bacterial survival in vitro (Figure 6). Altogether, this study demonstrates for the first time that the two non-canonical L-cysteine synthases have non-redundant biological functions. Deletion or biochemical inhibition of CysM or CysK2 perturbs redox homeostasis of *Mtb* and allow for the maximal effect of host macrophages antibacterial response, and thus increased elimination of virulent *Mtb*.

Methods

Bacterial strains and culturing conditions

Mtb culturing conditions were performed as described previously [5, 48].

Generation of *RvΔcysK2* mutant and complementation strain.

We generated gene replacement mutants through the recombineering method [49] as previously described [5, 48]. Briefly, 671bp upstream of 176th nucleotide from 5' end (5' flank) and 643 bp downstream of 943rd nucleotide from 3' end (3' flank) of *cysK2* were PCR amplified from *Rv* genomic DNA using Phusion DNA polymerase (Thermo Scientific). The amplicons were digested with BstAPI and ligated with compatible hygromycin resistance (*hyg*^{r}) cassette and *oriE*+cosλ fragments [49], to generate the allelic exchange substrate (AES). AES was digested with SnaBI to release the LHS-*hyg*^{r}-RHS fragment, and the eluted fragment was electroporated into the recombineering proficient *Rv-ET* strain [5]. Multiple *hyg*^{r} colonies were examined by PCRs to screen for legitimate recombination at *cysK2* locus. *RvΔcysK2*, thus generated, was cured of pNit-ET through negative selection on LB Agar plates containing 2% sucrose. To generate the complementation strain, full length *cysK2* gene was PCR amplified from genomic DNA isolated from *Rv* as the template and Phusion DNA polymerase (ThermoFischer Scientific). The amplicon was digested with NdeI-HindIII (NEB), cloned into the corresponding sites in pNit-3F and the resultant plasmid was electroporated into *RvΔcysK2* to generate the *RvΔcysK2::cysK2* strain. *RvΔcysM* and *RvΔcysM::cysM* strains were generated in the lab previously [5] using a similar method [2].

Ex vivo infection experiments

Balb/c, C57BL/6 (B6), phox$^{-/-}$ (B6.129S6-Cybbtm1Din/J; JAX# 002365) or IFN-γ$^{-/-}$ (B6.129S7-Ifngtm1Ts/J; JAX#002287) mice were procured from The Jackson Laboratory. 4% thioglycolate (Hi-Media) was injected into the peritoneum cavity of 4- to 6-weeks old mice and peritoneal macrophages were extracted four days post-injection and seeded and processed as described [5]. In specific cases, the peritoneal macrophages were treated with 10 ng/ml IFNγ (BD Biosciences) overnight and 10 ng/ml lipopolysaccharide (LPS, Sigma) for 2 h for activation. Where indicated, cells were further pretreated with 100 μM 1400 W (Sigma) overnight to inhibit iNOS or pretreated with 0.2 mM L-cysteine before infection. Single-cell *Mtb* suspensions were used for infection at 1:10 (host cells: bacteria) MOI. 4 h post-infection (p.i), cells were washed thrice and replenished with complete RPMI containing IFNγ + LPS, 1400 W, or L-cysteine, as required. The infected host cells were washed thrice with PBS, lysed using 0.05% Dodecyl sulfate sodium salt (SDS), and serial dilutions were plated on 7H11-OADC to enumerate bacillary survival.

***In vivo* infection experiments**

Mice (4–6-weeks) housed in ventilated cages at the Tuberculosis Aerosol Challenge Facility at the International Centre for Genetic Engineering and Biotechnology (New Delhi, India) were infected via aerosol route with ~100 bacilli using the Madison Aerosol Chamber (University of Wisconsin, Madison, WI). At 24 h post-infection, mice (n=2; per group) were euthanized to determine the bacterial deposition. At 4/8 weeks p.i, lungs and spleen were homogenized and plated on 7H11+OADC containing PANTA.

RNA isolation and qRT–PCRs

Mtb strains were cultured in triplicates in 7H9-ADS till O.D. reached 0.3-0.4. One set was left untreated (control), the other was treated with 50 μM of CHP for 6 h. A culture equivalent to 10 $O.D._{600}$ was resuspended in TRIzol (Invitrogen). Zirconium beads were added to the cell-Trizol mix to facilitate lysing *Mtb* cells with the help of a bead beater (MP FastPrep system, MP Biomedicals) and RNA was extracted and analyzed as described [5]. Data was plotted as $2^{(-\Delta\Delta Ct)}$ wherein the gene expression was normalized with respect to 16s rRNA (*rrs* gene), followed by normalization with control strain/condition/group.

RNA sequencing and analysis

Total RNA was isolated from two-three biological replicates of indicated *Mtb* strains, and their concentrations were checked by Qubit (ThermoFischer Scientific) followed by quality assessment through Agilent 2100 BioAnalyzer (Agilent RNA 6000 Nano Kit). Both sets of RNA seq represented in Figures 1 and 5 were processed and run at the same time, the same set of control (*Rv*) triplicates were used for the analysis of both figures. Samples with RIN values $\geq$ 7 were processed for RNA sequencing using the Illumina NovaSeq 6000 Platform (CSIR-CCMB central facility; read length of 100 bp, 20 million paired-end reads / sample).

Illumina adapters and low-quality reads were discarded and those with quality scores < 20 and smaller than 36 bp were eliminated from raw sequencing reads using cutadapt [50]. Processed reads were mapped to the *Mtb* H37Rv, (https://ftp.ncbi.nlm.nih.gov/genomes/refseq/bacteria/Mycobacterium_tuberculosis/reference/GCF_000195955.2_ASM19595v2/), using hisat2 with default parameters [51]. Uniquely aligned reads were counted with the help of feature Counts of Subread package [52] and those with total read count < 10 across all the samples were removed, and the rest were used for further downstream analysis. Differentially expressed genes (DEGs) were identified using DESeq2 [53] and those with adjusted p-value < 0.05 and absolute $\log_2$ Fold change >1 or 0.5 were considered. The raw read counts were rlog normalized the raw read counts for PCA plot and heat map with the

DESeq2 package.

Functional enrichment analysis

Functional enrichment analysis was performed with DAVID web services [54]. We specifically used GO terms and KEGG pathways for this analysis. Only top 10 enriched hits based on gene counts were plotted.

Preparation of samples for metabolomics.

Mtb strains were grown in 7H9 media until an OD 1 and then inoculated onto 0.22um nitrocellulose filters and grown on 7H10 plates containing 0.5g/L BSA Fraction V, 0.2% dextrose and 0.085% NaCl (ADS) for 5 days. The filters were then transferred to 7H10 plus ADS plates containing sodium sulfate-^{34}S (Merck 718882) containing either 50uM CHP or no CHP for 24 and 48 h. The metabolites were extracted by mechanical lysis in cold acetonitrile/methanol/water (2:2:1) containing 0.1mm acid washed Zirconia beads. The lysates were clarified by centrifugation and filtered through a 0.22um Spin-X column (Costar). The lysates were mixed 1:1 with acidified acetonitrile (0.1% formic acid). Due to the tendency of *M. tuberculosis* to form clamps, which significantly skew any cell number estimations we normalized samples to protein/peptide concentration using the BCA assay kit (Thermo). Therefore, our LC-MS data is express as ion counts/mg protein or ratios of that for the same metabolite. This is a standard way to express ion abundance data [10, 12].

Liquid chromatography – mass spectrometry metabolomics.

LC–MS analysis was done in an Agilent 1290 Infinity II HPLC connected to a 6230B time-of-flight (ToF) mass spectrometer using a Dual AJS ESI ionization source. Compounds were separated in a Cogent Diamond Hydride Type C silica column (2.1 × 150 mm). Solvent A was LC–MS grade H2O + 0.1% (v/v) formic acid and solvent B was acetonitrile + 0.1% (v/v) formic acid. The gradient was from 85% B to 5% B over 14 min. Flow rate was 0.4 mL/min. The ion source parameters were as follows: Gas temperature 250 °C, Drying gas flow rate 13 l/min, nebulizer pressure 35 psig, sheath gas temperature 350 °C, sheath gas flow 12 l/min, capillary voltage 3500 V and nozzle voltage 2000 V, The ion optic voltages were 110 V for the fragmentor, 65 V for the skimmer and 750 for the octopole radio frequency voltage. MS data were analyzed with the MassHunter suite version B0.7.0.00.

MIC analysis

MIC values were assessed using Alamar Blue assay, as described previously [55]. Briefly, 100µl 7H9-ADS medium without Tween 80 was added to each well of a 96-well plate. First well of each column were filled with 100µl of the test drug/antibiotic, which was then serially diluted across the column. *Mtb* cells corresponding to 0.01 A_{600} were diluted in 100µl 7H9-ADS medium and were added to each well. Two rows one in which the drug was not added (no drug [ND]), and the other wherein *Mtb* cells were replaced with 7H9-ADS (no cells [NC]) acted as controls. The 96 well plate was sealed with parafilm and kept at 37°C. After 5 days, 20µl of 0.25% filter-sterilized resazurin was added to each well, and color development was captured after 24 h.

Statistical analysis

Unless otherwise specified, experiments were performed in triplicates and repeated independently at least twice. CFU results were plotted, and significance of the datasets was calculated using one-way ANOVA followed by a *post hoc* test (Tukey test) on GraphPad Prism 5. Figures were customized using Adobe Illustrator version 26.3.1. Statistical significance was set at Pvalues < 0.05 significant (*, $P < 0.05$; **, $P < 0.005$; ***, $P < 0.0005$). Source datasets can be requested from the corresponding author.

Data availability

RNA Seq data is available at the NCBI Gene Expression Omnibus Database, accession no. GEO GSE225792, the link to the database is https://www.ncbi.nlm.nih.gov/geo/query/acc.cgi?acc=GSE225792 and the reviewer token for private access is ipmnekailfmlbcj.

Acknowledgements

We thank Dr. Apruva Sarin for *phox*$^{-/-}$ mice and thoughtful discussion; ICGEB for access to their TACF; CCMB for access to their sequencing facility. MZK was supported by Research Associateship from SERB (CRG/2018/001294). Research reported in this publication was supported by the core grant of the National Institute of Immunology; DBT grant BT/PR13522/COE/34/27/2015; SERB grant CRG/2018/001294, and JC Bose fellowship JCB/2019/000015 to VKN. Work in LPSC's laboratory was supported by the Francis Crick Institute, which receives its core funding from Cancer Research UK Grant FC001060, UK MRC Grant FC001060, and Wellcome Trust Grant FC001060.

Author contributions

MZK, LPSC and VKN conceptualized the study; MZK contributed to generation of constructs and strains; BS and MZK were involved in the preparation of RNA sequencing samples, while NKS and DTS performed the analyses. MZK and BS performed animal studies at ICGEB; MZK contributed to *in vitro* stress susceptibility assays, macrophage assays and inhibitor studies; DMH and LPSC performed the metabolomic studies; DVSP and DS synthesized chemical inhibitors; MZK curated the data. MZK, YK, LPSC and VKN wrote the manuscript; VKN and LPSC acquired funding for the study. All authors read and approved the manuscript.

Ethics statement

Protocols for animal experiments were preapproved by the Animal Ethics Committee of the National Institute of Immunology, New Delhi, India (IAEC numbers 409/16 and 462/18) as per standard institutional guidelines.

Figure Legends

Fig 1 | Non-canonical L-cysteine synthases facilitate mycobacterial survival upon host-like induced stresses *in vitro.* **(a)** 5-way Venn diagram highlighting DEGs belonging to sulfur metabolism pathway under indicated stress conditions (absolute $\log_2$ Fold change$\geq$ 0.5 and P_{adj} value <0.05). **(b)** Line Diagram illustrating the *cysK2* loci in *Rv* and *RvΔcysK2* and the strategy employed for the replacement of *cysK2* with *hyg*^{r}. Primer sets used for confirming the generation of *RvΔcysK2* are indicated as arrows. The first agarose gel image shows PCR amplicons with a control (*sigB*) gene-specific primer indicating the presence of nearly equivalent amount of genomic DNA isolated from *Rv* and *RvΔcysK2.* The second panel shows PCR amplicons with gene-specific primer set (F1-R1) in *Rv* and *RvΔcysK2* mutant, the third panel shows amplicons (F2-R2) expected only in *RvΔcysK2* mutant, and the fourth panel shows amplicons (F2-R3) in *Rv* and *RvΔcysK2* mutant confirming legitimate recombination at native loci. Mr represents 1-kb gene ruler ladder. **(c-i)** *Rv*, *RvΔcysM*, *RvΔcysK2*, *RvΔcysM::cysM*, and *RvΔcysK2*::*cysK2* strains were inoculated in Sauton's (c), PBS (d) or acidic (e), oxidative 50 µM Cumene hydroperoxide (CHP) for 24 h ((f), nitrosative (g), reductive (h) and SDS (i). Bar graphs represent the bacillary survival with data point indicating values CFU $\log_{10}$/mL $\pm$ standard deviations (SD) from individual replicate (n=3). Statistical significance was drawn in comparison with *Rv* using one-way ANOVA followed by a *post hoc* test (Tukey test; GraphPad prism). $^{**}P < 0.005$; $^{***}P < 0.0005$.

Fig 2 | *Distinct roles of CysM and CysK2 in attuning cellular processes.*

(a) PCA plot demonstrating separation of various bacterial strains under different conditions **(b-e)** Volcano plots illustrating significantly upregulated (blue) and downregulated (red) genes in indicated strains and conditions with absolute $\log_2$ Fold change$\geq$ 1 and P_{adj} value <0.05. Numbers in the top quadrant highlight the number of significantly upregulated (blue) and downregulated (red) genes in each condition **(f)** Venn diagram showing the number of significantly downregulated and upregulated DEGs that overlap between indicated strains **(g)** Heat Maps depicting normalized gene count of differentially expressed genes (DEGs) in independent replicates of *RvΔcysM* and *RvΔcysK2* grown under oxidative conditions with absolute $\log_2$ Fold change$\geq$ 1 and P_{adj} value <0.05. The colour intensity indicates relative upregulated (blue) and downregulated (red) genes compared to the control. **(h)** Horizontal bar graph depicting the number of DEGs belonging to a particular functional category upon oxidative stress in *RvΔcysM* compared to *RvΔcysK2* under oxidative conditions. **(i)** Pathway enrichment by DAVID depicting significantly enriched Gene Ontology (GO) biological processes based on DEGs upon oxidative stress in *RvΔcysM* compared to *RvΔcysK2* (absolute $\log_2$ Fold change>1 and Padj<0.05).

Fig 3 | *Key metabolites are differentially affected upon CysM and CysK2 deletion*

(a-d) Total abundance (Ion count/Protein concentration) of L-methionine (a), ergothioneine (b), mycothiol (c), and mycothione (d) in *Rv* with or without 50 μM CHP treatment. **(e-g)** The percentage of labelled (colored) and unlabeled (black) ergothioneine (e), mycothiol (f), and mycothione (g) in *Rv* with or without 50 μM CHP treatment at 48 h. Percentage was calculated with respect to 0 h abundance for each replicate. Bars depict the mean of biological replicates (n=3), and error bars represent the standard deviation. The same samples were used for analysis (a-d) and (e-g). Statistical significance was calculated between *Rv* and *RvΔcysM/ RvΔcysK2*; and between *RvΔcysM* and *RvΔcysK2* using non-parametric t-test. * $P < 0.05$; ** $P < 0.005$; *** $P < 0.0005$.

Fig 4 | L-cysteine synthases ameliorate mycobacterial survival in response to host-induced oxidative and nitrosative stress

(a) Pictorial representation of peritoneal macrophage infection experiments. Thioglycolate was injected into the peritoneum cavity of C57BL/6, phox$^{-/-}$, IFNγ$^{-/-}$ mice. Four days post-injection, peritoneal macrophages were extracted and activated by treatment with IFNγ overnight and LPS - 2 h prior to the infection. In specific cases, iNOS inhibitor 1400 W was added along with IFNγ/LPS. The intracellular bacillary survival was calculated 96 h p.i. **(b)** Peritoneal macrophages from C57BL/6 mice were infected, and intracellular bacillary survival was enumerated 96 h p.i. (c) Peritoneal macrophages from C57BL/6 mice were infected, left untreated (control) or treated with 0.2mM L-cysteine at the time of infection and intracellular bacillary survival was assessed 96 h p.i. **(d-f)** Peritoneal macrophages isolated from mice of indicated genotypes were either left untreated or treated with iNOS inhibitor, 1400W. Intracellular bacillary survival was enumerated 96 h p.i. **(b-f)** Data points are presented as CFU $\log_{10}$/ml ± SD of each replicate (n=3). Statistical significance was drawn in comparison with *Rv* using one-way ANOVA followed by a *post hoc* test (Tukey test; GraphPad prism). ** $P < 0.005$; *** $P < 0.0005$.

Fig 5 | Deletion of non-canonical L-cysteine synthases attenuates mycobacterial survival in murine lungs and spleen

(a) Schematic outline of murine infection experiment. C57BL/6 ($n = 12$ per group) were infected with *Rv*, *RvΔcysM*, or *RvΔcysM::cysM* strains via an aerosol route. CFU was enumerated at day 1 (n=2), week 4 (n=5) and week 8 (n=5). **(b-c)** Each data point represents Log_{10} CFU in lung (b) and spleen (c) of an infected animal, and the error bar indicates the median with interquartile range for each group. **(d)** Schematic outline of murine infection experiment. C57BL/6 ($n = 12$ per group) were infected with *Rv*, *RvΔcysK2*, or *RvΔcysK2::cysK2* strains via an aerosol route. CFU was

enumerated at day 1 (n=2), week 4 (n=5) and week 8 (n=5). **(e-f)** Each data point represents Log_{10} CFU in the lung (e) and spleen (f) of an infected animal, and the error bar indicates the median with interquartile range for each group. **(g)** Schematic outline of murine infection experiment. C57BL/6 ($n = 7$ per group), phox$^{-/-}$ ($n = 7$ per group), IFNγ$^{-/-}$ ($n = 7$ per group) were infected with *Rv*, *RvΔcysM*, or *RvΔcysM::cysM* strains via an aerosol route. CFU was enumerated at day 1 (n=2) and week 4 (n=5). (h-i) Each data point represents Log_{10} CFU in the lung **(h)** and spleen **(i)** of an infected animal, and the error bar indicates the median with interquartile range for each group. **(a-i)** Statistical significance was drawn in comparison with *Rv* using one-way ANOVA followed by a *post hoc* test (Tukey test; GraphPad prism). ***$P < 0.0005$.

Fig 6 | L-*cysteine synthases inhibitors can effectively kill Mtb* within the host.

(a) Chemical structure and formula of lead compounds. **(b).** Venn diagram illustrating the specificity of compounds on mycobacterial L-cysteine synthases. **(c).** Peritoneal macrophages were infected with *Rv*. 4 h post-infection, cells were either left untreated (control) or 5 mg/ml C1 (a), C2 (b) or C3 (c) was added to the infected cells. Bar graphs represent mean Log_{10} CFU/ml ± SD, and values from independent replicates are represented by individual data points (n=3). **(d-f).** Alamar blue assay is used to determine MIC values of C1 (d), C2, and C3 (f) with and without Isoniazid in *Rv*. Starting concentration of INH in 1A is 0.96 μg/ml, 1B-0.43 μg/ml and each subsequent column 2 fold dilution. Concentration of C1, C2 and C3 were 2.4 mg/ml in 2A and 1.2 mg/ml in 2B and in each subsequent column 2 fold dilution. The concentration of INH + C1 or C2 in 3A was 0.015 μg/ml + 0.15 mg/ml, and 3B was 0.0075 μg/ml + 0.075 mg/ml. and each subsequent column 2-fold dilution. The concentration of INH + C3 in 3A was .015 μg/ml + 37 μg/ml, and 3B was 0.0075 μg/ml + 18.5 and each subsequent column 2-fold dilution. ND-no drug and NC- no culture.

Supplementary Figure 1 | Overview of Sulfur metabolism pathway in *Mycobacterium tuberculosis*

Sulfate is imported via the sulfate transporter composed of SufI.CysT.W.A, which is acted upon by CysDNC complex to form Adenosine-5'-phosphosulfate (APS). APS can either form sulfolipids or is reduced by subsequent actions of CysH and SirA to form sulfide. CysK1, the classical L-cysteine synthase, utilizes reduced sulfide and O-acetyl-L-serine as substrates to form L-Cysteine. Alternatively, L-cysteine is produced by CysM, a non-canonical L-cysteine synthase that is unique to actinomycetes and uses O-phospho-L-serine and a small sulfur carrier protein CysO to form L-cysteine. *Mtb* also encodes for a third L-cysteine synthase, CysK2. However, the major product of this pathway is S-sulfo-L-cysteine, which can get rapidly converted to L-cysteine. The reverse transsulfuration pathway is also depicted.

Supplementary Figure 2 | *Sulfur assimilation and L-cysteine biosynthesis pathways are upregulated under stress conditions.*

(a-e) Volcano plots illustrating significantly upregulated (blue) and downregulated (red) genes in *Rv* grown under indicated conditions with Log_2 Fold change$\geq$ 1 and P_{adj} value <0.05 compared to control (untreated) *Rv*. Numbers in the top quadrant depict the number of significantly upregulated (blue) and downregulated (red) genes in each condition compared to the control. **(f-j)** Heat Maps depicting normalized gene count of differentially expressed genes (DEGs) in independent replicates of *Rv* grown under indicated conditions with Log_2 Fold change$\geq$ 1 and P_{adj} value <0.05. The colour intensity indicates relative upregulated (blue) and downregulated (red) genes compared to the control.

Supplementary Figure 3 | Genes that were differentially expressed in at least one of the five stresses.

We compiled a list of genes differentially expressed in at least one of the five stresses against compared untreated *Rv*. We made a data frame of fold changes for these selected genes in the five comparisons. We then generated a heatmap where the five comparisons were plotted as columns (x-axis), and selected genes were plotted as rows (y-axis). Hierarchical clustering was performed on the y-axis so that genes with similar fold changes across comparisons clustered together.

Supplementary Figure 4 | *Genes belonging to the Sulfur metabolism pathway are upregulated upon oxidative stress*

(a) Horizontal bar graph demonstrating the number of DEGs belonging to a particular functional category under indicated stress condition. **(b-e)** Pathway enrichment by DAVID depicting significantly enriched Gene Ontology (GO) biological processes based on DEGs in starvation (b), SDS (c), Nitrosative (d) and pH 5.5 (e). **(f)** Pathway enrichment by DAVID depicting significantly

affected Gene Ontology (GO) biological processes based on DEGs (Log_2 Fold change$\geq$ 0.5 and P_{adj} value <0.05).

Supplementary Figure 5 | L-cysteine synthases facilitate mycobacterial survival upon oxidative stresses *in vitro*

(a-c) *Rv*, *RvΔcysM*, *RvΔcysK2*, *RvΔcysM::cysM*, and *RvΔcysK2::cysK2* strains were inoculated in 7H9-ADC (a), 7H9-ADS (b), 7H9-ADS plus 10mM diamide (c) medium. Bar graphs represent the bacillary survival with data point indicating values CFU log_{10}/mL $\pm$ SD from individual replicate (n=3). Statistical significance was drawn in comparison with *Rv* using one-way ANOVA followed by a *post hoc* test (Tukey test; GraphPad prism). $^{**}P < 0.005$; $^{***}P < 0.0005$.

Supplementary Figure 6 | Unique transcriptional signatures of CysM and CysK2.

(a & c) Volcano plots illustrating significantly upregulated (blue) and downregulated (red) genes in indicated strains and conditions with Log_2 Fold change> 1 and P_{adj} value <0.05. Numbers in the top quadrant highlight the number of significantly upregulated (blue) and downregulated (red) genes in each condition **(b & d)** Heat Maps depicting normalized gene count of differentially expressed genes (DEGs) in independent replicates of *RvΔcysM* and *RvΔcysK2* compared to *Rv* with Log_2 Fold change> 1 and P_{adj} value <0.05. The colour intensity indicates relative upregulated (blue) and downregulated (red) genes compared to the control. **(e)** Venn diagram showing the number of significantly downregulated and upregulated DEGs that overlap between indicated strains (Log_2 Fold change> 1 and P_{adj} value <0.05). **(f & g)** Pathway enrichment by DAVID depicting significantly enriched Gene Ontology (GO) biological processes based on DEGs upon oxidative stress in *RvΔcysM* (f) and *RvΔcysK2* (g) compared to *Rv* (Log_2 Fold change> 1 and P_{adj} value <0.05).

Supplementary Figure 7 | Overview of metabolites tracked through ^{35}S sulfur incorporation

Table S1: Differentially Expressed Genes (DEG) analysis *Rv* under stress vs *Rv*.

Table S2: We compiled a list of differentially expressed genes in at least one of the five comparisons against control.

Table S3: Pathway enrichment analysis of DEGs from Table S1.

Table S3: DEG analysis of RvΔcysM or RvΔcysK2 vs Rv with or without CHP stress & DEG analysis RvΔcysM +CHP vs RvΔcysK2 + CHP.

Table S4: Pathway enrichment analysis of DEGs from Table S3.

References

1. Hampshire, T., et al., *Stationary phase gene expression of Mycobacterium tuberculosis following a progressive nutrient depletion: a model for persistent organisms?* Tuberculosis (Edinb), 2004. **84**(3-4): p. 228-38.
2. Manganelli, R., et al., *Role of the extracytoplasmic-function sigma factor sigma(H) in Mycobacterium tuberculosis global gene expression.* Mol Microbiol, 2002. **45**(2): p. 365-74.
3. Pinto, R., et al., *The Mycobacterium tuberculosis cysD and cysNC genes form a stress-induced operon that encodes a tri-functional sulfate-activating complex.* Microbiology (Reading), 2004. **150**(Pt 6): p. 1681-1686.
4. Schnappinger, D., et al., *Transcriptional Adaptation of Mycobacterium tuberculosis within Macrophages: Insights into the Phagosomal Environment.* J Exp Med, 2003. **198**(5): p. 693-704.
5. Khan, M.Z., et al., *Redox homeostasis in Mycobacterium tuberculosis is modulated by a novel actinomycete-specific transcription factor.* EMBO J, 2021. **40**(14): p. e106111.
6. Rengarajan, J., B.R. Bloom, and E.J. Rubin, *Genome-wide requirements for Mycobacterium tuberculosis adaptation and survival in macrophages.* Proc Natl Acad Sci U S A, 2005. **102**(23): p. 8327-32.
7. Wooff, E., et al., *Functional genomics reveals the sole sulphate transporter of the Mycobacterium tuberculosis complex and its relevance to the acquisition of sulphur in vivo.* Mol Microbiol, 2002. **43**(3): p. 653-63.
8. McAdam, R.A., et al., *In vivo growth characteristics of leucine and methionine auxotrophic mutants of Mycobacterium bovis BCG generated by transposon mutagenesis.* Infect Immun, 1995. **63**(3): p. 1004-12.
9. Urbanek, R., et al., *Oral immunotherapy with grass pollen in enterosoluble capsules. A prospective study of the clinical and immunological response.* Eur J Pediatr, 1990. **149**(8): p. 545-50.
10. Mougous, J.D., et al., *Sulfotransferases and sulfatases in mycobacteria.* Chem Biol, 2002. **9**(7): p. 767-76.
11. Schnell, R., et al., *Siroheme- and [Fe4-S4]-dependent NirA from Mycobacterium tuberculosis is a sulfite reductase with a covalent Cys-Tyr bond in the active site.* J Biol Chem, 2005. **280**(29): p. 27319-28.
12. Pinto, R., et al., *Sulfite reduction in mycobacteria.* J Bacteriol, 2007. **189**(18): p. 6714-22.
13. Qiu, J., et al., *Identification and characterization of serine acetyltransferase encoded by the Mycobacterium tuberculosis Rv2335 gene.* Int J Mol Med, 2013. **31**(5): p. 1229-33.
14. Schnell, R., et al., *Structural insights into catalysis and inhibition of O-acetylserine sulfhydrylase from Mycobacterium tuberculosis. Crystal structures of the enzyme alpha-aminoacrylate intermediate and an enzyme-inhibitor complex.* J Biol Chem, 2007. **282**(32): p. 23473-81.
15. Agren, D., et al., *Cysteine synthase (CysM) of Mycobacterium tuberculosis is an O-phosphoserine sulfhydrylase: evidence for an alternative cysteine biosynthesis pathway in mycobacteria.* J Biol Chem, 2008. **283**(46): p. 31567-74.
16. O'Leary, S.E., et al., *O-phospho-L-serine and the thiocarboxylated sulfur carrier protein CysO-COSH are substrates for CysM, a cysteine synthase from Mycobacterium tuberculosis.* Biochemistry, 2008. **47**(44): p. 11606-15.
17. Jurgenson, C.T., et al., *Crystal structure of a sulfur carrier protein complex found in the cysteine biosynthetic pathway of Mycobacterium tuberculosis.* Biochemistry, 2008. **47**(39): p. 10354-64.
18. Burns, K.E., et al., *Reconstitution of a new cysteine biosynthetic pathway in Mycobacterium tuberculosis.* J Am Chem Soc, 2005. **127**(33): p. 11602-3.
19. Steiner, E.M., et al., *CysK2 from Mycobacterium tuberculosis is an O-phospho-L-serine-dependent S-sulfocysteine synthase.* J Bacteriol, 2014. **196**(19): p. 3410-20.
20. Nakamura, T., H. Iwahashi, and Y. Eguchi, *Enzymatic proof for the identity of the S-sulfocysteine synthase and cysteine synthase B of Salmonella typhimurium.* J Bacteriol, 1984. **158**(3): p. 1122-7.
21. Zhang, Y.J., et al., *Tryptophan biosynthesis protects mycobacteria from CD4 T-cell-mediated killing.* Cell, 2013. **155**(6): p. 1296-308.
22. Dwivedy, A., et al., *De novo histidine biosynthesis protects Mycobacterium tuberculosis from host IFN-gamma mediated histidine starvation.* Commun Biol, 2021. **4**(1): p. 410.

23. Hatzios, S.K. and C.R. Bertozzi, *The regulation of sulfur metabolism in Mycobacterium tuberculosis.* PLoS Pathog, 2011. **7**(7): p. e1002036.
24. Senaratne, R.H., et al., *5'-Adenosinephosphosulphate reductase (CysH) protects Mycobacterium tuberculosis against free radicals during chronic infection phase in mice.* Mol Microbiol, 2006. **59**(6): p. 1744-53.
25. Betts, J.C., et al., *Evaluation of a nutrient starvation model of Mycobacterium tuberculosis persistence by gene and protein expression profiling.* Mol Microbiol, 2002. **43**(3): p. 717-31.
26. Voskuil, M.I., et al., *The response of mycobacterium tuberculosis to reactive oxygen and nitrogen species.* Front Microbiol, 2011. **2**: p. 105.
27. Voskuil, M.I., K.C. Visconti, and G.K. Schoolnik, *Mycobacterium tuberculosis gene expression during adaptation to stationary phase and low-oxygen dormancy.* Tuberculosis (Edinb), 2004. **84**(3-4): p. 218-27.
28. Brunner, K., et al., *Profiling of in vitro activities of urea-based inhibitors against cysteine synthases from Mycobacterium tuberculosis.* Bioorg Med Chem Lett, 2017. **27**(19): p. 4582-4587.
29. Manganelli, R., et al., *The Mycobacterium tuberculosis ECF sigma factor sigmaE: role in global gene expression and survival in macrophages.* Mol Microbiol, 2001. **41**(2): p. 423-37.
30. de Carvalho, L.P., et al., *Metabolomics of Mycobacterium tuberculosis reveals compartmentalized co-catabolism of carbon substrates.* Chem Biol, 2010. **17**(10): p. 1122-31.
31. Sao Emani, C., et al., *The DeltaCysK(2) mutant of Mycobacterium tuberculosis is sensitive to vancomycin associated with changes in cell wall phospholipid profile.* Biochem Biophys Res Commun, 2022. **624**: p. 120-126.
32. Agapova, A., et al., *Flexible nitrogen utilisation by the metabolic generalist pathogen Mycobacterium tuberculosis.* Elife, 2019. **8**.
33. Vilcheze, C., et al., *Altered NADH/NAD+ ratio mediates coresistance to isoniazid and ethionamide in mycobacteria.* Antimicrob Agents Chemother, 2005. **49**(2): p. 708-20.
34. Buchmeier, N.A., G.L. Newton, and R.C. Fahey, *A mycothiol synthase mutant of Mycobacterium tuberculosis has an altered thiol-disulfide content and limited tolerance to stress.* J Bacteriol, 2006. **188**(17): p. 6245-52.
35. Buchmeier, N.A., et al., *Association of mycothiol with protection of Mycobacterium tuberculosis from toxic oxidants and antibiotics.* Mol Microbiol, 2003. **47**(6): p. 1723-32.
36. Rawat, M., et al., *Mycothiol-deficient Mycobacterium smegmatis mutants are hypersensitive to alkylating agents, free radicals, and antibiotics.* Antimicrob Agents Chemother, 2002. **46**(11): p. 3348-55.
37. Rawat, M., et al., *Comparative analysis of mutants in the mycothiol biosynthesis pathway in Mycobacterium smegmatis.* Biochem Biophys Res Commun, 2007. **363**(1): p. 71-6.
38. Saini, V., et al., *Ergothioneine Maintains Redox and Bioenergetic Homeostasis Essential for Drug Susceptibility and Virulence of Mycobacterium tuberculosis.* Cell Rep, 2016. **14**(3): p. 572-585.
39. Sassetti, C.M., D.H. Boyd, and E.J. Rubin, *Comprehensive identification of conditionally essential genes in mycobacteria.* Proc Natl Acad Sci U S A, 2001. **98**(22): p. 12712-7.
40. Curran, F.T. and G.L. Hill, *Symptomatic colitis in the anal canal after restorative proctocolectomy.* Aust N Z J Surg, 1992. **62**(12): p. 941-3.
41. Sareen, D., et al., *Mycothiol is essential for growth of Mycobacterium tuberculosis Erdman.* J Bacteriol, 2003. **185**(22): p. 6736-40.
42. Huet, G., M. Daffe, and I. Saves, *Identification of the Mycobacterium tuberculosis SUF machinery as the exclusive mycobacterial system of [Fe-S] cluster assembly: evidence for its implication in the pathogen's survival.* J Bacteriol, 2005. **187**(17): p. 6137-46.
43. Huet, G., et al., *Protein splicing of SufB is crucial for the functionality of the Mycobacterium tuberculosis SUF machinery.* J Bacteriol, 2006. **188**(9): p. 3412-4.
44. Buchmeier, N. and R.C. Fahey, *The mshA gene encoding the glycosyltransferase of mycothiol biosynthesis is essential in Mycobacterium tuberculosis Erdman.* FEMS Microbiol Lett, 2006. **264**(1): p. 74-9.
45. Raman, K., K. Yeturu, and N. Chandra, *targetTB: a target identification pipeline for Mycobacterium tuberculosis through an interactome, reactome and genome-scale structural analysis.* BMC Syst Biol, 2008. **2**: p. 109.

46. Brunner, K., et al., *Inhibitors of the Cysteine Synthase CysM with Antibacterial Potency against Dormant Mycobacterium tuberculosis.* J Med Chem, 2016. **59**(14): p. 6848-59.
47. Schnell, R., D. Sriram, and G. Schneider, *Pyridoxal-phosphate dependent mycobacterial cysteine synthases: Structure, mechanism and potential as drug targets.* Biochim Biophys Acta, 2015. **1854**(9): p. 1175-83.
48. Khan, M.Z., et al., *Protein kinase G confers survival advantage to Mycobacterium tuberculosis during latency-like conditions.* J Biol Chem, 2017. **292**(39): p. 16093-16108.
49. van Kessel, J.C. and G.F. Hatfull, *Recombineering in Mycobacterium tuberculosis.* Nat Methods, 2007. **4**(2): p. 147-52.
50. Martin, M., *Cutadapt removes adapter sequences from high-throughput sequencing reads.* 2011, 2011. **17**(1): p. 3.
51. Kim, D., et al., *Graph-based genome alignment and genotyping with HISAT2 and HISAT-genotype.* Nat Biotechnol, 2019. **37**(8): p. 907-915.
52. Liao, Y., G.K. Smyth, and W. Shi, *featureCounts: an efficient general purpose program for assigning sequence reads to genomic features.* Bioinformatics, 2014. **30**(7): p. 923-30.
53. Love, M.I., W. Huber, and S. Anders, *Moderated estimation of fold change and dispersion for RNA-seq data with DESeq2.* Genome Biol, 2014. **15**(12): p. 550.
54. Sherman, B.T., et al., *DAVID: a web server for functional enrichment analysis and functional annotation of gene lists (2021 update).* Nucleic Acids Res, 2022. **50**(W1): p. W216-21.
55. Khan, M.Z. and V.K. Nandicoori, *Deletion of pknG Abates Reactivation of Latent Mycobacterium tuberculosis in Mice.* Antimicrob Agents Chemother, 2021. **65**(4).

Figure 1

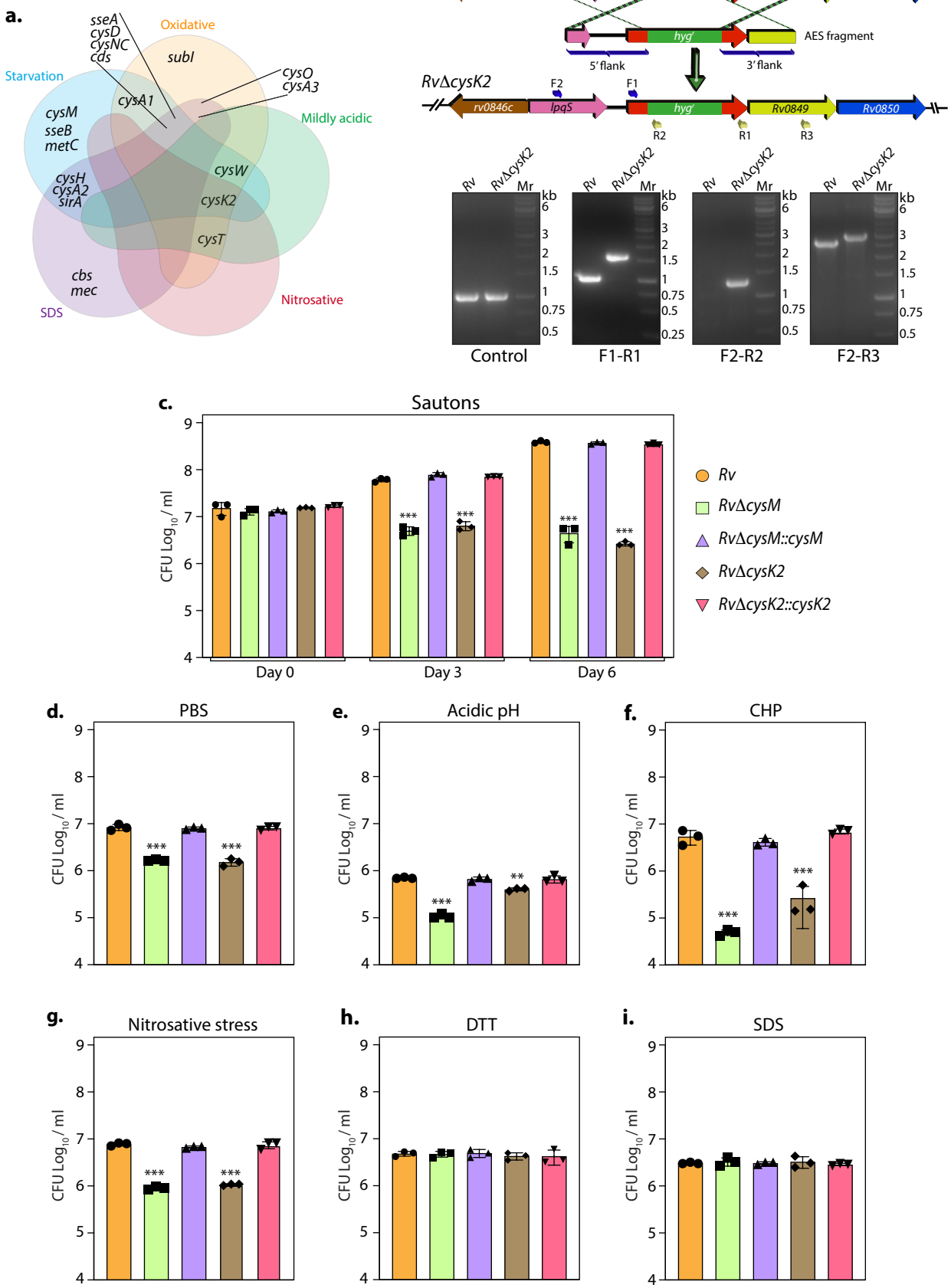
a.
Oxidative
Starvation
Mildly acidic
Nitrosative
SDS
sseA
cysD
cysNC
cds
subI
cysO
cysA3
cysA1
cysM
sseB
metC
cysW
cysH
cysA2
sirA
cysK2
cysT
cbs
mec
b.
Rv
rv0846c
lpqS
cysK2
Rv0849
Rv0850
hyg^r
AES fragment
5' flank
3' flank
RvΔcysK2
F2
F1
R2
R1
R3
Rv
RvΔcysK2
Mr
kb
Control
F1-R1
F2-R2
F2-R3
c.
Sautons
CFU Log10 / ml
Day 0
Day 3
Day 6
Rv
RvΔcysM
RvΔcysM::cysM
RvΔcysK2
RvΔcysK2::cysK2
d.
PBS
e.
Acidic pH
f.
CHP
g.
Nitrosative stress
h.
DTT
i.
SDS

Figure 2

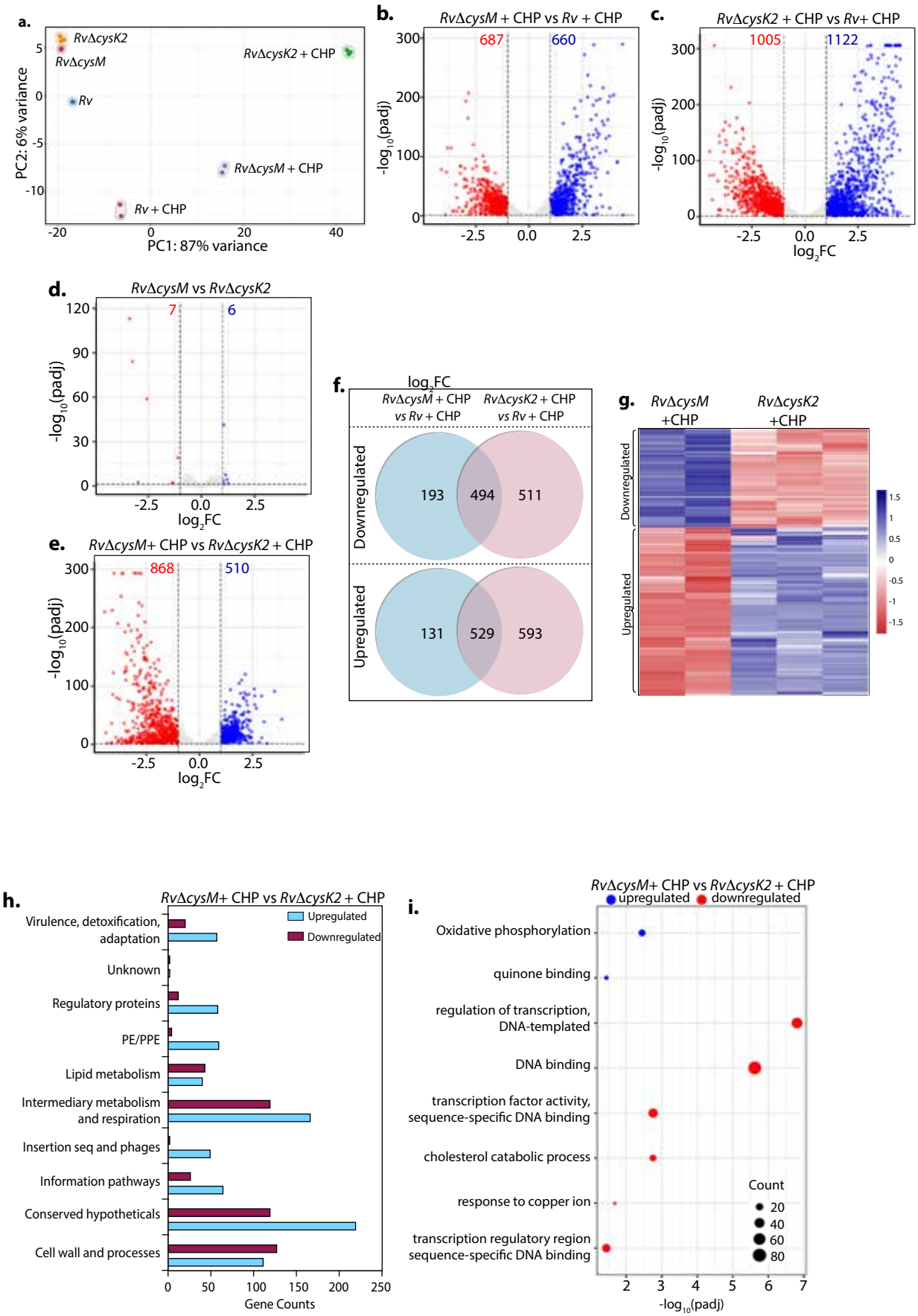
a.
RvΔcysK2
RvΔcysM
RvΔcysK2 + CHP
Rv
RvΔcysM + CHP
Rv + CHP
PC2: 6% variance
PC1: 87% variance
b.
RvΔcysM + CHP vs Rv + CHP
687
660
-log10(padj)
log2FC
c.
RvΔcysK2 + CHP vs Rv+ CHP
1005
1122
-log10(padj)
log2FC
d.
RvΔcysM vs RvΔcysK2
7
6
-log10(padj)
log2FC
e.
RvΔcysM+ CHP vs RvΔcysK2 + CHP
868
510
-log10(padj)
log2FC
f.
log2FC
RvΔcysM + CHP vs Rv + CHP
RvΔcysK2 + CHP vs Rv + CHP
Downregulated
193
494
511
Upregulated
131
529
593
g.
RvΔcysM +CHP
RvΔcysK2 +CHP
Downregulated
Upregulated
h.
RvΔcysM+ CHP vs RvΔcysK2 + CHP
Upregulated
Downregulated
Virulence, detoxification, adaptation
Unknown
Regulatory proteins
PE/PPE
Lipid metabolism
Intermediary metabolism and respiration
Insertion seq and phages
Information pathways
Conserved hypotheticals
Cell wall and processes
Gene Counts
i.
RvΔcysM+ CHP vs RvΔcysK2 + CHP
upregulated
downregulated
Oxidative phosphorylation
quinone binding
regulation of transcription, DNA-templated
DNA binding
transcription factor activity, sequence-specific DNA binding
cholesterol catabolic process
response to copper ion
transcription regulatory region sequence-specific DNA binding
Count
20
40
60
80
-log10(padj)

Figure 3

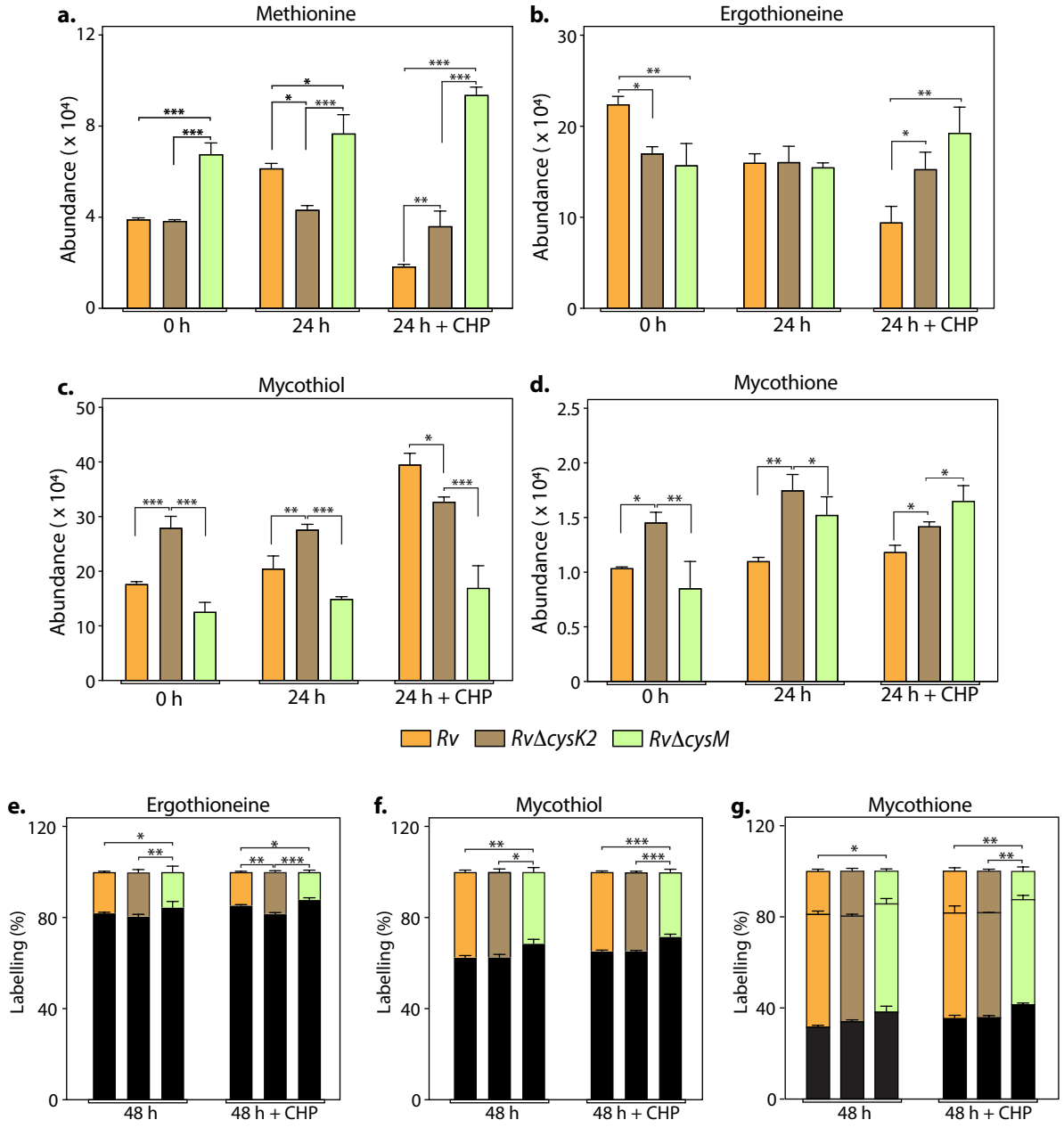
a.
Methionine
Abundance (x 10⁴)
0 h
24 h
24 h + CHP
b.
Ergothioneine
c.
Mycothiol
d.
Mycothione
Rv
RvΔcysK2
RvΔcysM
e.
Ergothioneine
Labelling (%)
48 h
48 h + CHP
f.
Mycothiol
g.
Mycothione

Figure 4

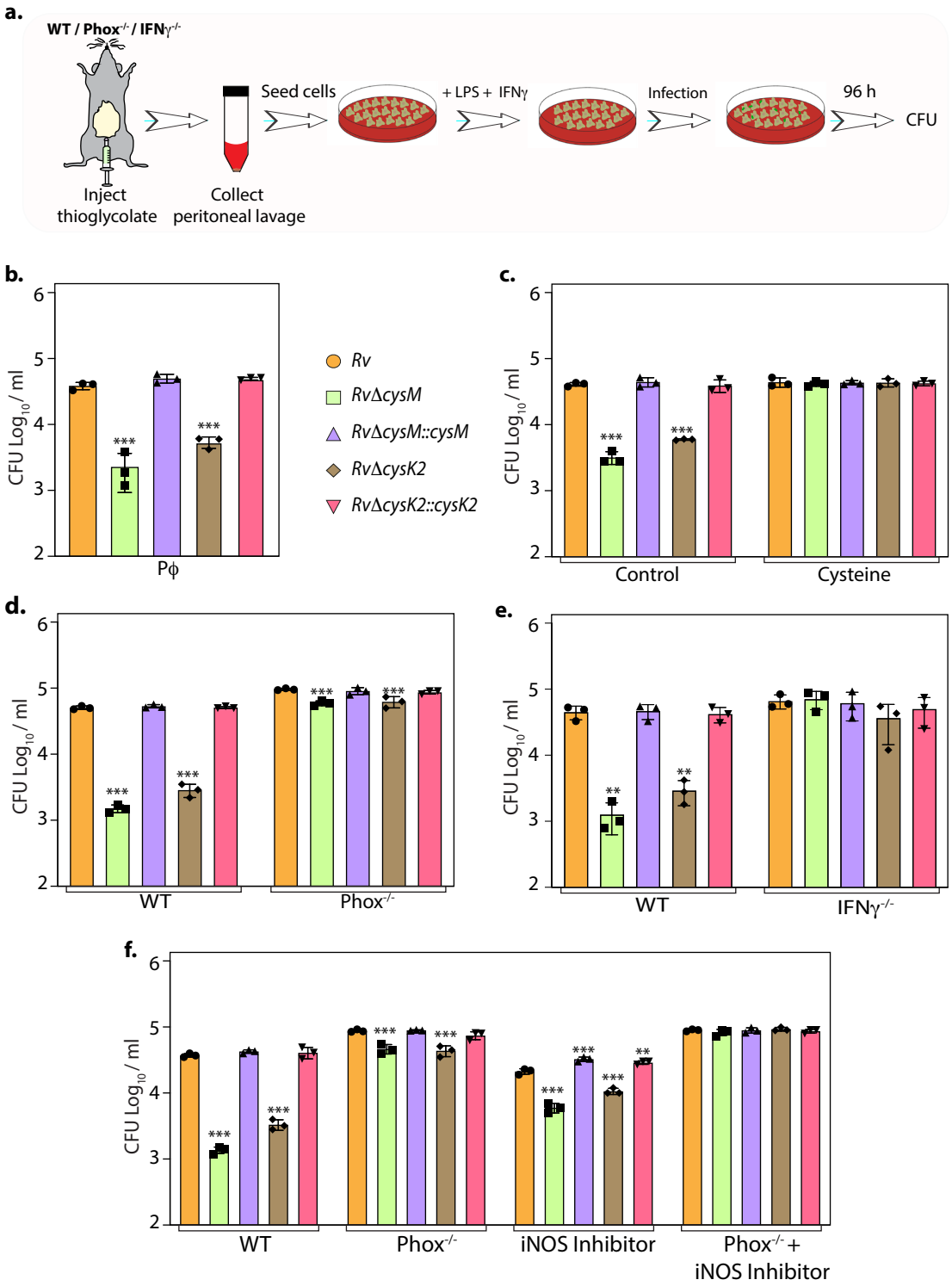
a.
WT / Phox-/- / IFNγ-/-
Inject thioglycolate
Collect peritoneal lavage
Seed cells
+ LPS + IFNγ
Infection
96 h
CFU
b.
c.
d.
e.
f.
CFU Log10 / ml
Rv
RvΔcysM
RvΔcysM::cysM
RvΔcysK2
RvΔcysK2::cysK2
Pϕ
Control
Cysteine
WT
Phox-/-
IFNγ-/-
iNOS Inhibitor
Phox-/- + iNOS Inhibitor

Figure 5

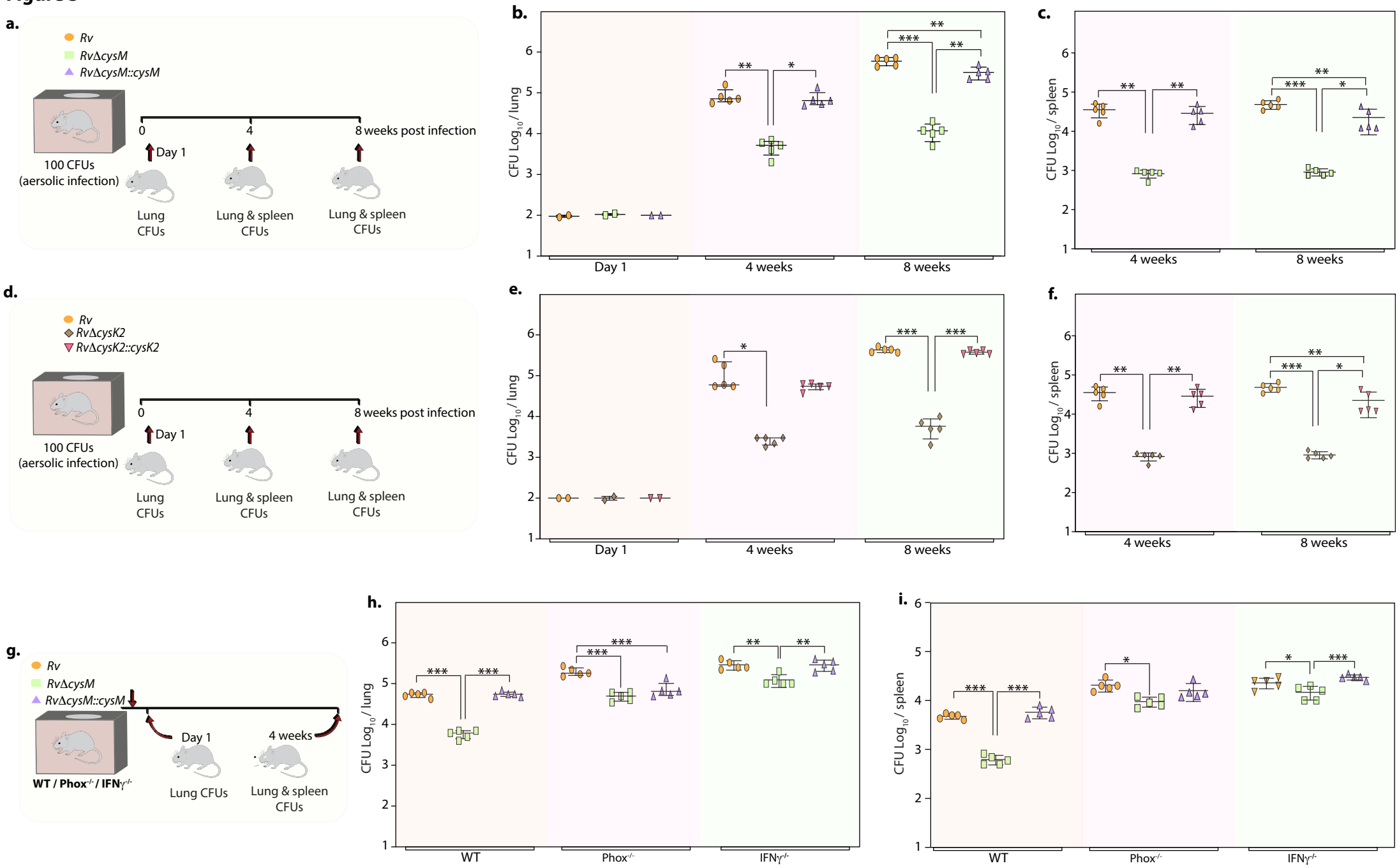
a.
Rv
RvΔcysM
RvΔcysM::cysM
0
4
8 weeks post infection
Day 1
100 CFUs
(aersolic infection)
Lung
CFUs
Lung & spleen
CFUs
Lung & spleen
CFUs
b.
CFU Log10 / lung
Day 1
4 weeks
8 weeks
c.
CFU Log10 / spleen
4 weeks
8 weeks
d.
Rv
RvΔcysK2
RvΔcysK2::cysK2
0
4
8 weeks post infection
Day 1
100 CFUs
(aersolic infection)
Lung
CFUs
Lung & spleen
CFUs
Lung & spleen
CFUs
e.
CFU Log10 / lung
Day 1
4 weeks
8 weeks
f.
CFU Log10 / spleen
4 weeks
8 weeks
g.
Rv
RvΔcysM
RvΔcysM::cysM
Day 1
4 weeks
WT / Phox-/- / IFNγ-/-
Lung CFUs
Lung & spleen
CFUs
h.
CFU Log10 / lung
WT
Phox-/-
IFNγ-/-
i.
CFU Log10 / spleen
WT
Phox-/-
IFNγ-/-

Figure 6

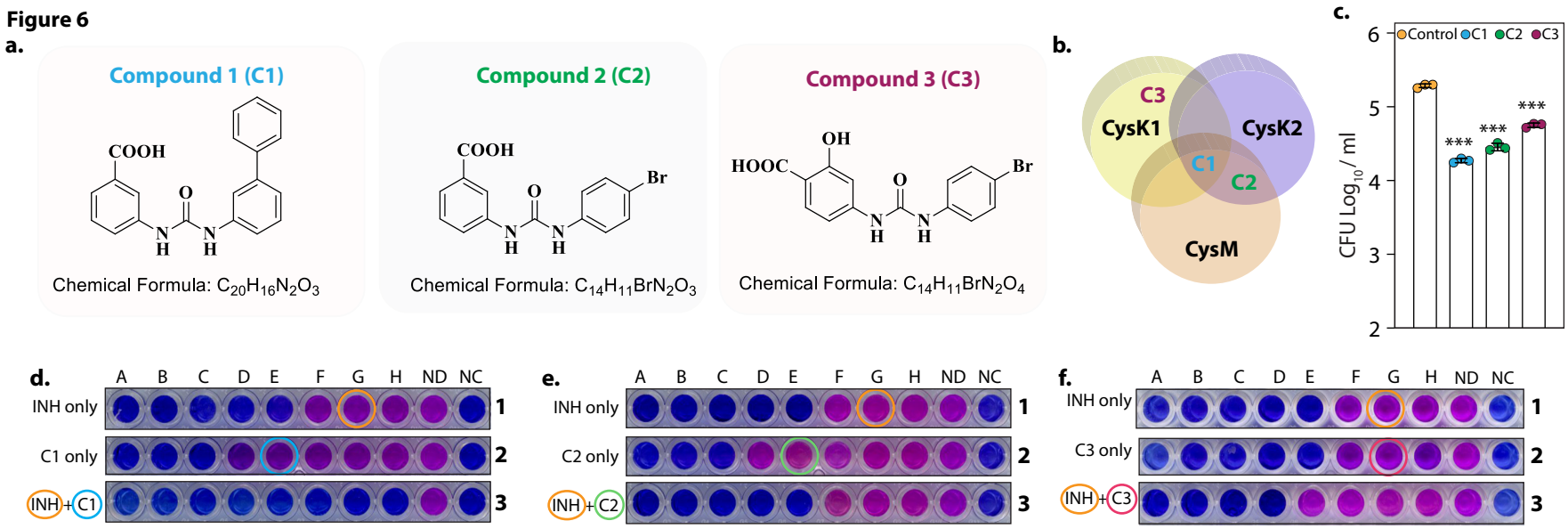
a.
Compound 1 (C1)
COOH
O
N H
N H
Chemical Formula: $C_{20}H_{16}N_2O_3$
Compound 2 (C2)
COOH
O
Br
N H
N H
Chemical Formula: $C_{14}H_{11}BrN_2O_3$
Compound 3 (C3)
OH
HOOC
O
Br
N H
N H
Chemical Formula: $C_{14}H_{11}BrN_2O_4$
b.
C3
CysK1
CysK2
C1
C2
CysM
c.
Control C1 C2 C3
CFU Log_{10} / ml
6
5
4
3
2
***
d.
A B C D E F G H ND NC
INH only
C1 only
INH + C1
1
2
3
e.
A B C D E F G H ND NC
INH only
C2 only
INH + C2
1
2
3
f.
A B C D E F G H ND NC
INH only
C3 only
INH + C3
1
2
3

Figure S1

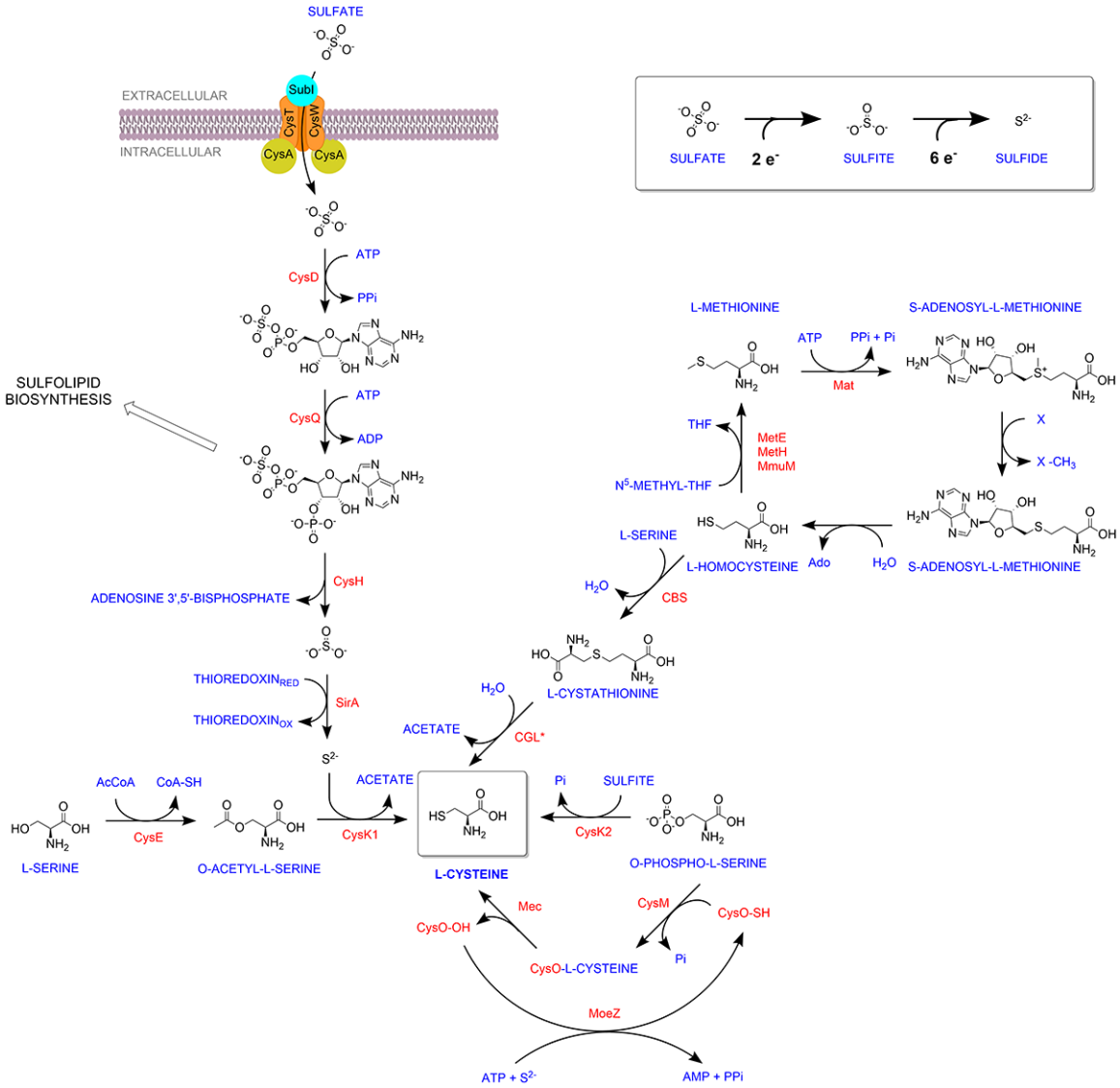
SULFATE
EXTRACELLULAR
INTRACELLULAR
SubI
CysT
CysW
CysA
CysA
ATP
CysD
PPi
SULFOLIPID BIOSYNTHESIS
ATP
CysQ
ADP
CysH
ADENOSINE 3',5'-BISPHOSPHATE
THIOREDOXIN$_{RED}$
SirA
THIOREDOXIN$_{OX}$
S^{2-}
AcCoA
CoA-SH
CysE
L-SERINE
O-ACETYL-L-SERINE
ACETATE
CysK1
L-CYSTEINE
Pi
SULFITE
CysK2
O-PHOSPHO-L-SERINE
H_2O
ACETATE
CGL*
L-CYSTATHIONINE
L-SERINE
H_2O
CBS
L-HOMOCYSTEINE
Ado
H_2O
S-ADENOSYL-L-METHIONINE
X
X -CH_3
S-ADENOSYL-L-METHIONINE
ATP
PPi + Pi
Mat
L-METHIONINE
THF
MetE
MetH
MmuM
N^5-METHYL-THF
CysO-OH
Mec
CysO-L-CYSTEINE
CysM
Pi
CysO-SH
MoeZ
ATP + S^{2-}
AMP + PPi
SULFATE
2 e$^-$
SULFITE
6 e$^-$
SULFIDE
S^{2-}

Figure S2

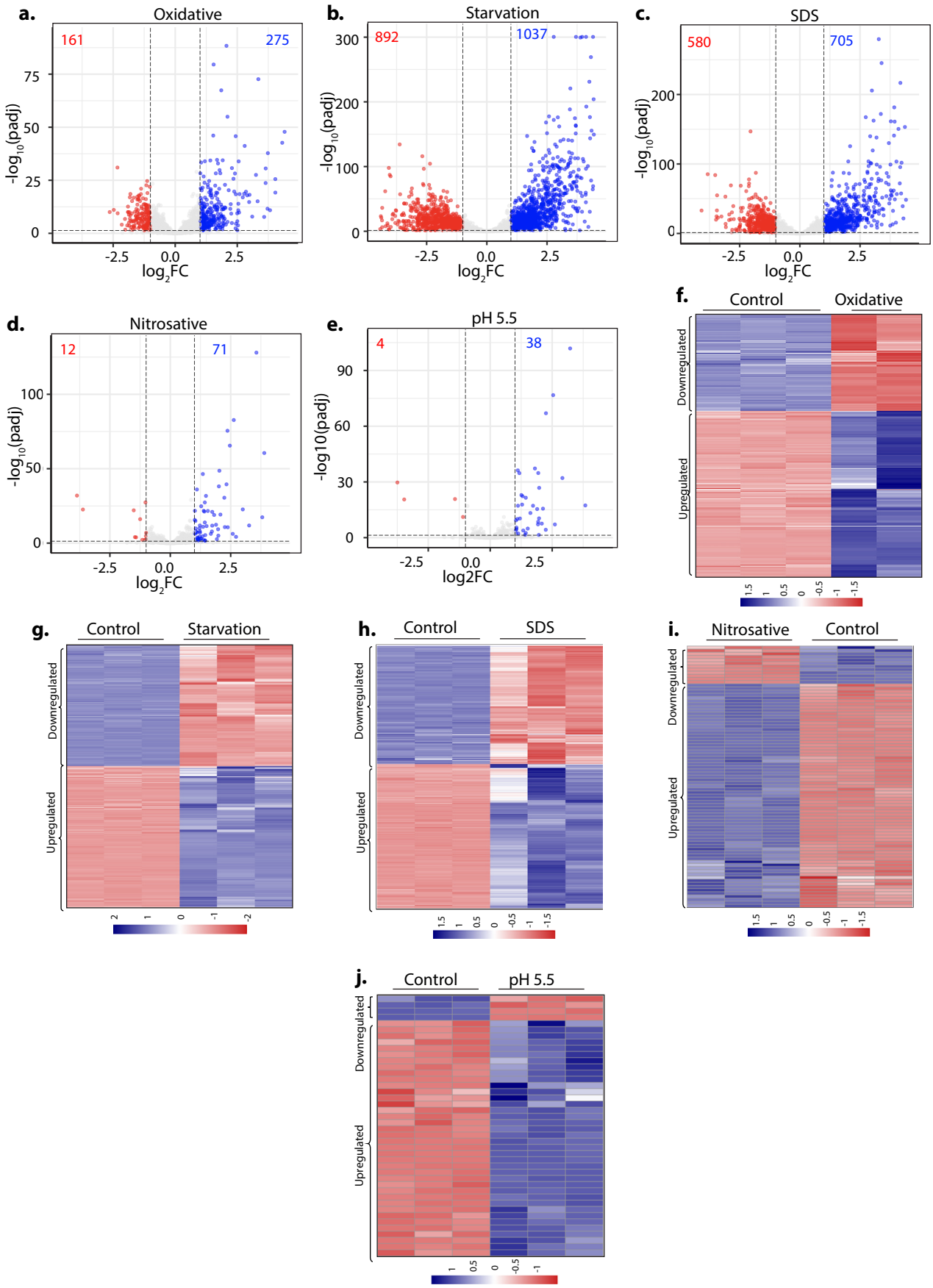
a.
Oxidative
161
275
-log10(padj)
log2FC
b.
Starvation
892
1037
c.
SDS
580
705
d.
Nitrosative
12
71
e.
pH 5.5
4
38
-log10(padj)
log2FC
f.
Control
Oxidative
Downregulated
Upregulated
g.
Control
Starvation
h.
Control
SDS
i.
Nitrosative
Control
j.
Control
pH 5.5

Figure S3

Figure S4

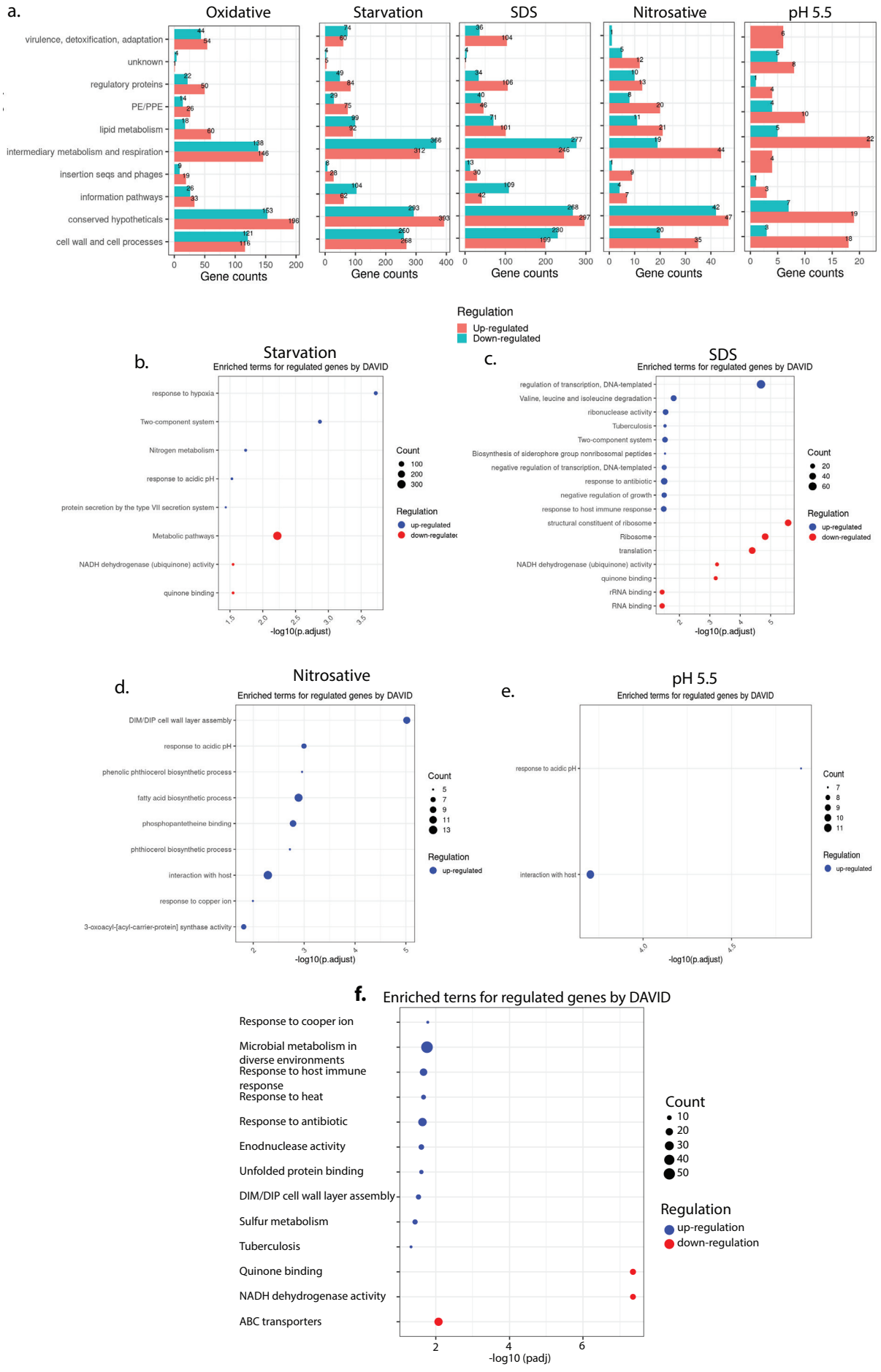
a.
Oxidative
Starvation
SDS
Nitrosative
pH 5.5
virulence, detoxification, adaptation
unknown
regulatory proteins
PE/PPE
lipid metabolism
intermediary metabolism and respiration
insertion seqs and phages
information pathways
conserved hypotheticals
cell wall and cell processes
Gene counts
Regulation
Up-regulated
Down-regulated
b.
Starvation
Enriched terms for regulated genes by DAVID
response to hypoxia
Two-component system
Nitrogen metabolism
response to acidic pH
protein secretion by the type VII secretion system
Metabolic pathways
NADH dehydrogenase (ubiquinone) activity
quinone binding
-log10(p.adjust)
Count
Regulation
up-regulated
down-regulated
c.
SDS
Enriched terms for regulated genes by DAVID
regulation of transcription, DNA-templated
Valine, leucine and isoleucine degradation
ribonuclease activity
Tuberculosis
Two-component system
Biosynthesis of siderophore group nonribosomal peptides
negative regulation of transcription, DNA-templated
response to antibiotic
negative regulation of growth
response to host immune response
structural constituent of ribosome
Ribosome
translation
NADH dehydrogenase (ubiquinone) activity
quinone binding
rRNA binding
RNA binding
-log10(p.adjust)
Count
Regulation
up-regulated
down-regulated
d.
Nitrosative
Enriched terms for regulated genes by DAVID
DIM/DIP cell wall layer assembly
response to acidic pH
phenolic phthiocerol biosynthetic process
fatty acid biosynthetic process
phosphopantetheine binding
phthiocerol biosynthetic process
interaction with host
response to copper ion
3-oxoacyl-[acyl-carrier-protein] synthase activity
-log10(p.adjust)
Count
Regulation
up-regulated
e.
pH 5.5
Enriched terms for regulated genes by DAVID
response to acidic pH
interaction with host
-log10(p.adjust)
Count
Regulation
up-regulated
f.
Enriched terms for regulated genes by DAVID
Response to cooper ion
Microbial metabolism in diverse environments
Response to host immune response
Response to heat
Response to antibiotic
Enodnuclease activity
Unfolded protein binding
DIM/DIP cell wall layer assembly
Sulfur metabolism
Tuberculosis
Quinone binding
NADH dehydrogenase activity
ABC transporters
-log10 (padj)
Count
Regulation
up-regulation
down-regulation

Figure S5

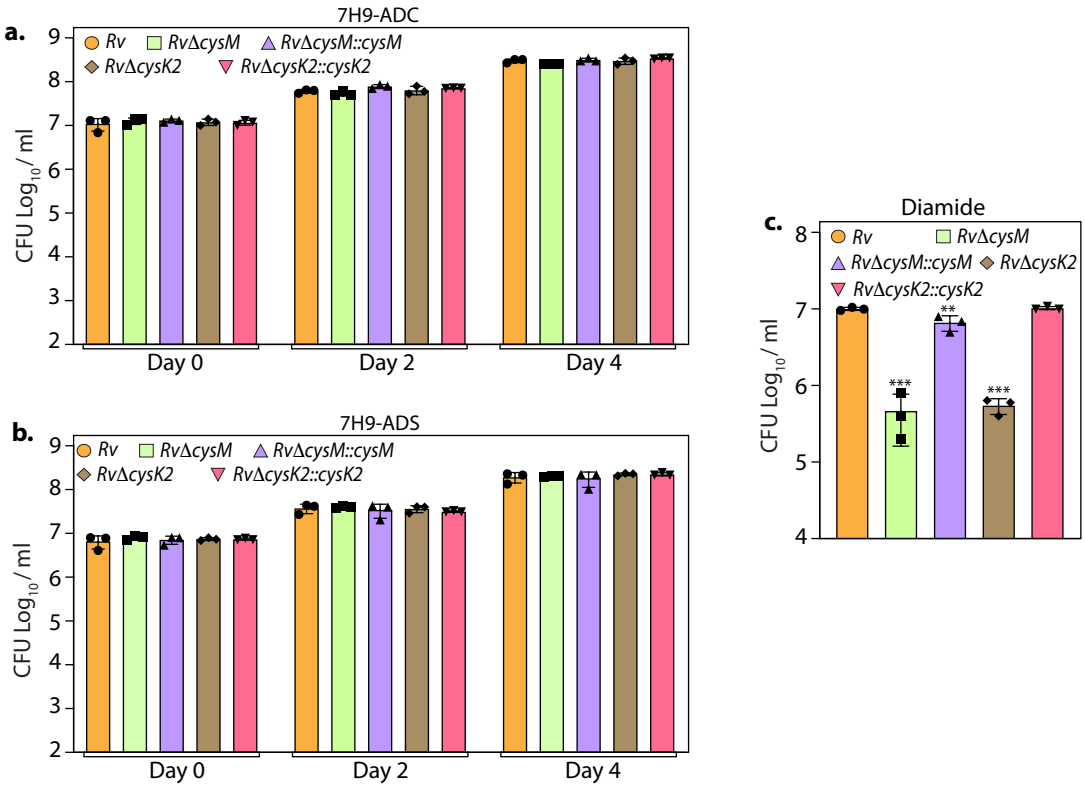
a.
7H9-ADC
Rv
RvΔcysM
RvΔcysM::cysM
RvΔcysK2
RvΔcysK2::cysK2
CFU Log10 / ml
Day 0
Day 2
Day 4
b.
7H9-ADS
Rv
RvΔcysM
RvΔcysM::cysM
RvΔcysK2
RvΔcysK2::cysK2
CFU Log10 / ml
Day 0
Day 2
Day 4
c.
Diamide
Rv
RvΔcysM
RvΔcysM::cysM
RvΔcysK2
RvΔcysK2::cysK2
CFU Log10 / ml
***
**
***

Figure S6

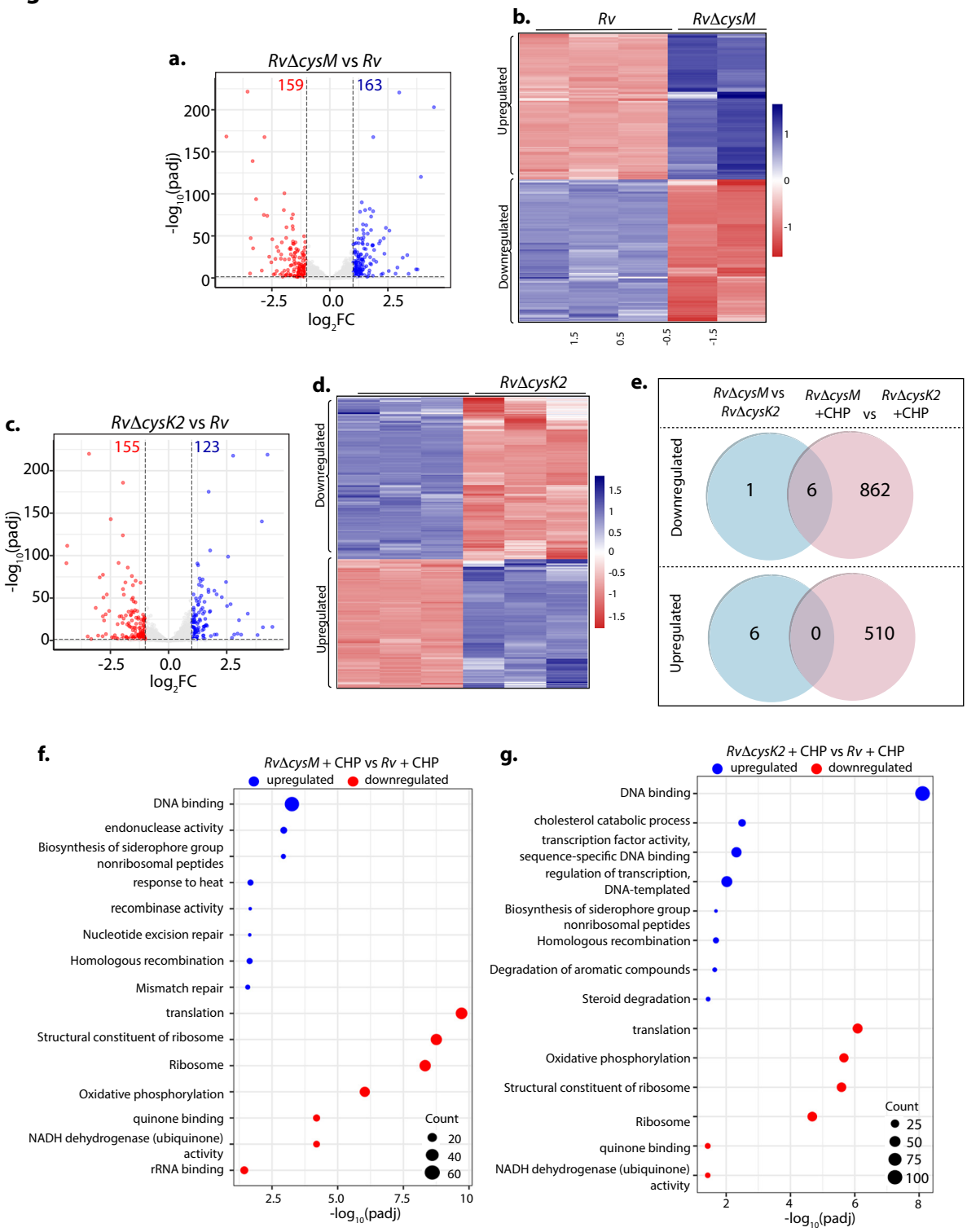
a.
RvΔcysM vs Rv
159
163
-log10(padj)
log2FC
b.
Rv
RvΔcysM
Upregulated
Downregulated
c.
RvΔcysK2 vs Rv
155
123
d.
RvΔcysK2
e.
RvΔcysM vs RvΔcysK2
RvΔcysM +CHP vs RvΔcysK2 +CHP
Downregulated
Upregulated
1
6
862
6
0
510
f.
RvΔcysM + CHP vs Rv + CHP
upregulated
downregulated
DNA binding
endonuclease activity
Biosynthesis of siderophore group nonribosomal peptides
response to heat
recombinase activity
Nucleotide excision repair
Homologous recombination
Mismatch repair
translation
Structural constituent of ribosome
Ribosome
Oxidative phosphorylation
quinone binding
NADH dehydrogenase (ubiquinone) activity
rRNA binding
Count
20
40
60
-log10(padj)
g.
RvΔcysK2 + CHP vs Rv + CHP
upregulated
downregulated
DNA binding
cholesterol catabolic process
transcription factor activity, sequence-specific DNA binding
regulation of transcription, DNA-templated
Biosynthesis of siderophore group nonribosomal peptides
Homologous recombination
Degradation of aromatic compounds
Steroid degradation
translation
Oxidative phosphorylation
Structural constituent of ribosome
Ribosome
quinone binding
NADH dehydrogenase (ubiquinone) activity
Count
25
50
75
100
-log10(padj)

Figure S7

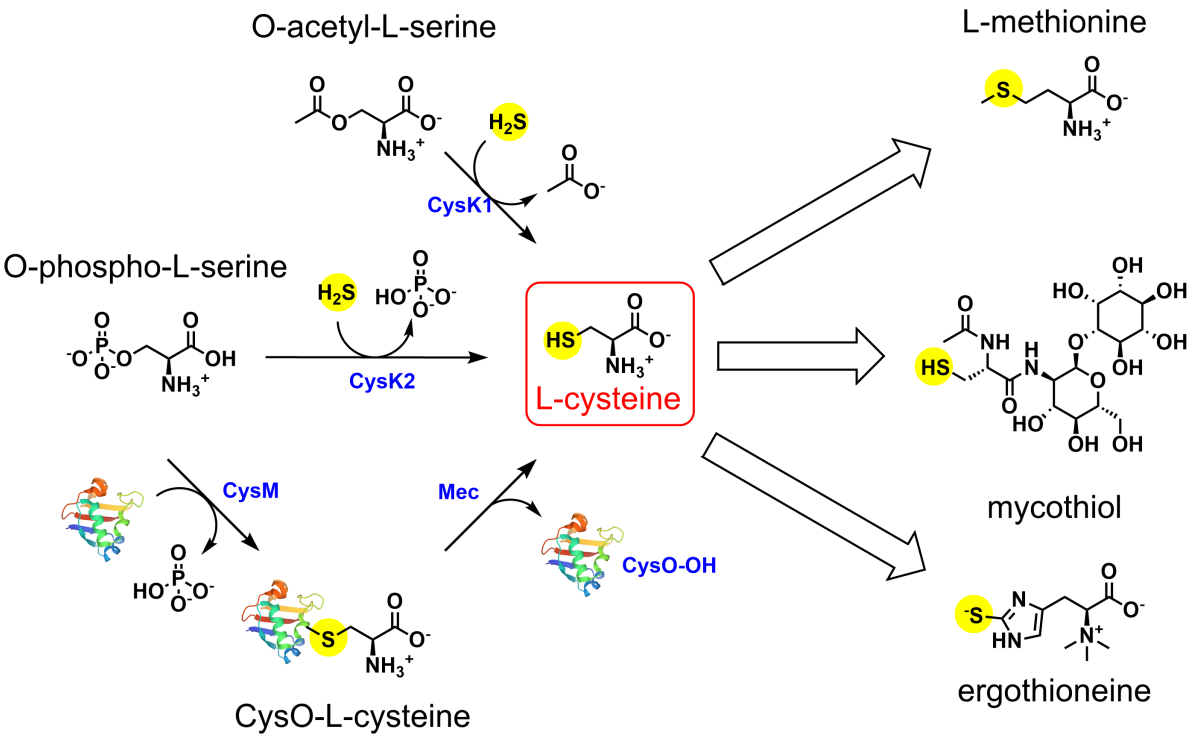
O-acetyl-L-serine
L-methionine
H_2S
CysK1
O-phospho-L-serine
H_2S
CysK2
L-cysteine
mycothiol
CysM
Mec
CysO-OH
CysO-L-cysteine
ergothioneine